UNIVERSITY OF CALIFORNIA,
IRVINE

Human Channel Modeling and Optimization for Intra-body Communication

THESIS

submitted in partial satisfaction of the requirements
for the degree of

MASTER OF SCIENCE

in Electrical and Computer Engineering

by

Ibrahim Nasser I Alquaydheb

Thesis Committee:
Professor Ahmed Eltawil, Chair
Professor Ender Ayanoglu
Professor Ozdal Boyraz

2018

DEDICATION

To

My dear grandmother and parents

TABLE OF CONTENTS

[1] The formulas and models presented in this section are imported from [1].
[2]This chapter's experiments are cooperative work with Ahmed E Khorshid.

LIST OF FIGURES

LIST OF TABLES

ACKNOWLEDGMENTS

I would like to express the deepest appreciation and gratitude to my advisor, Professor Ahmed Eltawil, for his exceptional guidance, motivation and support throughout this academic journey. His tremendous influence began since I have joined the Saudi Arabia international program of 2012 that raised my ambitions to be the best version of myself as an engineer which concluded by completing this work. Without his persistent help and thoughtful insight, this thesis would not have been possible.

I would like to thank Professor Ender Ayanoglu and Professor Ozdal Boyraz for being part of my thesis committee.

Very special thanks to Ahmed Eissa Khorshid, who is a good friend of mine and the lead researcher of IBC research group at the Electrical Engineering and Computer Science, University of California, Irvine. His extensive understanding, experience and continuous help have paved the way to start this research with the best background, knowledge and experiments setup. It would be impossible to reach this point of research without his guidance.

In addition, I would like to thank Sarkis Babikian at the Micro Integrated Devices and Systems Laboratory for his help in setting up the presented experiments in this thesis. Also special thanks to my friends Ahmed Alzughaibi, Umar Kazmi, Ahmed Mokhtar, Mohamed Fouda, Michael Ayoub, Sergey Shaboyan, Mohammad Almajhadi and Mohammed Alnemari for all of the support and encouragement that helped immensely to complete this degree.

Moreover, a message of recognition to Prince Sattam bin Abdulaziz University and to the Saudi Arabian Cultural Mission for all outstanding support. I would not be able to complete all of this achievement without their constant aid.

Finally, I consider myself very lucky and blessed to come from such an amazing and supportive family. My most sincere gratitude and thanks to my grandmother and parents. Also, to my twin brother Hisham for pushing each other to constantly improve ourselves. To all of my brothers and sisters for the unconditional love and encouragement.

ABSTRACT OF THE THESIS

Human Channel Modeling and Optimization for Intra-body Communication

By

Ibrahim Nasser I Alquaydheb

Master of Science in Electrical and Computer Engineering

University of California, Irvine, 2018

Professor Ahmed Eltawil, Chair

The desire to have ultra compact, low power, wearable and implanted biosensors/actuators encourages researchers to develop new communication methods that can replace current Radio Frequency (RF) wireless communication links. RF links require power and area hungry analog circuitry that limits the usability of such systems. This thesis conducts a thorough study on a promising technique called intra-body communication which utilizes the human body as a transmission medium, where galvanic coupling and capacitive coupling represent the main approaches to implement the intra-body communication (IBC) system.

IBCs literature review is presented showing the main motivation behind this research and the prior trials in the field, as well as highlighting the obstacles facing this technique. A circuit model is adopted to derive a transfer function that can capture the human channel properties to determine the transmission gain. Moreover, finite element method (FEM) technique is utilized to determine the path loss of the human channel, typically the human arm model, and to examine the current density distribution in human tissues using both a full and a reduced order model. In addition, the effect of bone fracture internal fixation implant effect on the channel parameters is investigated. Finally, to validate the FEM and circuit model, a fabricated human arm phantom is introduced in detail by covering the fabrication process, dielectric properties and transmission results.

Chapter 1

Introduction

1.1 Background

The increasing trend to improve health monitoring and lifestyle technologies has rapidly encouraged researches to focus on developing and innovating new applications to fulfill these demands. Continuous low-powered health monitoring techniques can promote health care by providing a real-time feedback to the user to adjust a certain behavior such as body posture. In addition, it can perform a continuous body diagnosis over a long time to detect early signs of any life threatening diseases by using body miniaturized sensors that are able to track, diagnose and detect vital signs (e.g. heart pulse acquired using Electrocardiogram (ECG), neural signals detected using electroencephalography (EEG), pH level and oxygen saturation).

So far, connectivity of most existing biosignal sensors to remote monitors in addition to wearable visual and audio entertainment devices to data sink applications, e.g. virtual reality (VR) headset, is accomplished using data cables which forms a body area network (BAN). Dispensing connecting cables by establishing a wireless radio frequency (RF) link,

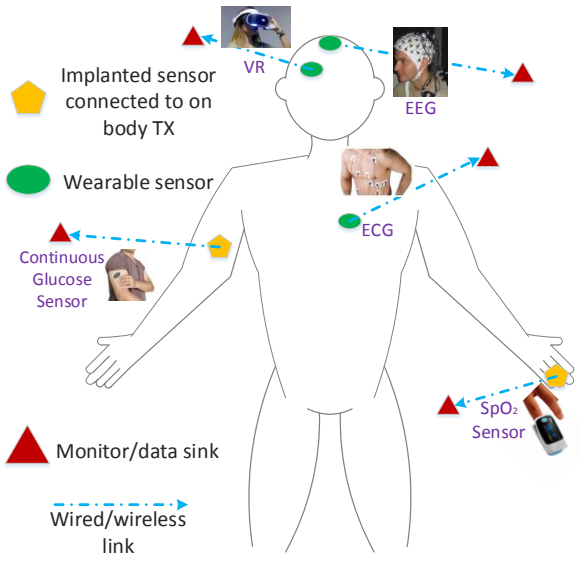

Figure 1.1: Wired or wireless wearable or implanted biosignal detection devices including EEG[2], VR[3], ECG[4], Continuous Glucose monitor[5] and SpO_2 measurement display[6].

known as wireless body area network (WBAN) as shown in figure 1.1, offers more movement flexibility and freedom for a wide spectrum of users, e.g. long-term monitoring of patients with chronic disease which can be critical for some cases such as children with attention deficit hyperactivity disorder. Moreover, wireless monitoring systems and medical tools may revolutionize the outcome of medical surgeries to be less invasive, shorter in time and less complex for surgeons which lead to higher surgical success rate, in other words less error. Furthermore, WBANs promote user identity authentication systems that rely on capturing biometric readings (such as ECG and EEG user profile) and wirelessly transmitting the data to a base station for further data processing and identification [12].

By determining the targeted data rate of each health care and lifestyle sensors and applications, the validity of initiating a wireless link becomes applicable. Table 1.1 summarizes the targeted channel data rate and minimum desired battery life of multiple biomedical and multimedia applications. Due to the nature of biosignals that oscillate at low frequencies which do not exceed 42 Hz [13][14], the required bit rate to transmit biosignals is in the order of few kb/s. In addition, some of the available hearing aid devices utilize the mini-

Table 1.1: System requirements for common BAN applications [11].

	Data rate target	**Desired battery life**
12-Channels ECG	72 kb/s (Sampling freq 500 Hz, 12-bit ADC)	>1 week
24-Channels EEG	86.4 kb/s (Sampling freq 300 Hz, 12-bit ADC)	>1 week
Hearing aid	200 kb/s	>40 Hrs
Glucose, CO_2, O_2, temperature and pH monitoring	<10 kb/s	>1 week
Audio	1 Mb/s	>24 Hrs
Video	<10 Mb/s	>12 Hrs

mum audio sampling rate for the sake of increasing battery life which require a bit rate of 200 kb/s. However, BAN multimedia applications mainly focus on real-time video and high quality audio streaming which requires higher data rate at 1 Mb/s and 10 Mb/s for both applications, respectively.

Deploying WBAN for biomedical and lifestyle applications faces multiple key challenges that must be taken in consideration:

- Safety: Existing network shall meet the signal propagation regulations to ensure the safety of human subject and not interfere with biological signals.
- Power consumption: Mainly by increasing battery life of each sensor and device especially for implanted sensors.
- Bit rate: A scalable data rate up to 10 Mb/s is the transmission goal. However, a trade off to power efficiency has to considered.
- Security: WBAN security limitations call for implementing novel higher security techniques to ensure the confidentiality of user information.
- Design properties: The size, weight and shape of sensors must satisfy user comfort and comply with WBAN requirements.

Proprietary and standard wireless technologies have been used to interconnect WBAN sensors and devices which are standardized by the IEEE Task Group TG6 as IEEE 802.15.6 [15]. Table 1.2 reviews and compares the properties of classic and low-power bluetooth, ZigBee, ANT, Sensium and Zarlink(ZL70101) topologies.

Bluetooth standard offers sufficient bit rate and low cost with the option of ultra low power if using the developed low-power Bluetooth technique; Yet, all the other listed topologies incorporate lower power consumption with different data rates. ZigBee lower average power consumption is suitable for WBAN biosignal sensors due to the low-duty-cycle of required devices. However, low data rate limits ZigBee priority over other standards. ANT and Sensium are proprietary standards that are optimized for WBAN health care and lifestyle applications. ANT features higher data rate compared to Sensium and it enables user trade-off between data rate and power consumption. Nevertheless, Sensium adopts ultra-lower power consumption.

In contrast to all of the previous four technologies which is deployable for only wearable body sensor, Zarlink has developed a wireless implanted transceiver modeled as ZL70101. This system utilizes extremely low transmission power consumption which is suitable for implanted sensors due to the need for less frequent battery replacement.

Bluetooth, ZigBee, ANT and Sensium technologies operate at the overcrowded industrial, scientific, and medical (ISM) band, ranging from 902MHz-928MHz and 2400MHz-2500MHz, with a frequency spectrum centered at 868 MHz, 915 MHz for Sensium and at 2.4 GHz for the other standards resulting in coexistence, interference and severe performance degradation problems which is a real concern for critical continuous monitoring medical applications. Also, these operating frequencies are compatible with the narrow band (NB) physical layer (PHY) of IEEE 802.15.6 standard which encounters severe attenuation and shadowing effect when propagating through the human body [16]. In addition, inherent limited quality of service (QoS) of mentioned techniques encourages finding an alternative transmission method

Table 1.2: Characteristics summary of wireless technologies for BAN[11].

	Spectrum	**Channels**	**Data rate**	**Peak power**
Bluetooth (classic & low energy)	2.4 GHz	classic-79 low energy-3	classic (1-3 Mb/s) low energy(1 Mb/s)	classic (45mA@3.3V) low energy(28mA@3.3V)
ZigBee	2.4 GHz	16	250 kb/s	16.5 mA@1.8V
ANT	2.4 GHz	125	1 Mb/s	22 mA@3.3V
Sensium	868 MHz, 915MHz	16	50 kb/s	3 mA@1.2V
Zarlink(ZL70101)	402-405 MHz, 433-434 MHz	10	200-800 kb/s	5 mA@3.3V

that can fulfill and improve targeted system properties.

Accordingly, a new promising transmission technique referred to as intra-body communication (IBC) which uses the human body as a transmission channel has been investigated. This method may mitigate the disadvantages of previously mentioned standards by overcoming coexistence issues, improving transmission rate and decreasing energy consumption without compromising QoS. Moreover, IBC features intrinsic security, since the propagated signal is confined within the human body, and interconnection of wearable to implanted or implanted to implanted sensors.

1.2 Intra-body Communications Technique

Intra-body communication is a novel transmission topology that utilizes the human body as a transmission medium or a waveguide to connect wireless implanted or wearable sensors and actuators to other receiving or transmitting devices, typically co-located on the human body [17]. This technique uses the human channel to perform data exchange and transmitting between wearable-wearable, implanted- wearable and implanted-implanted sensors and actuators or to be exported to an external medical monitor for further medical assessment. Also, this channel may permit local real-time data streaming between external media applications and wearable wireless entertainment devices. The motivation behind the idea of linking WBANs using IBC comes from the high demand to develop on-body sensors, actuators and devices that comply with the trends of ultra-low power consumption, high data rate, security and coexistence. By fulfilling these network requirements, user convenience and enhanced ergonomic design of body devices are guaranteed.

The feasibility of establishing IBC channel results in developing multiple applications network that improve medical, lifestyle and entertainment applications. Figure 1.2 shows an example of a three layer network architecture that consists of WBAN, a base station and finally a database.

In this approach, the WBAN exploits IBC technique to transmit detected biosiganl or real-time streamed data. The configuration of the WBAN depends inherently on the required sensors application. The star, mesh and tree network setups are suitable for WBAN. The star network topology is the best choice for medical applications among these configurations since connecting different biosignal detecting sensors directly to one central node, as shown in figure 1.2, is short distance, one-hop wireless communication [18]. Considering the limitations of sensors' memory and power consumption, all collected data is transmitted to the coordinator node, processed and redirected to the targeted destination which could be

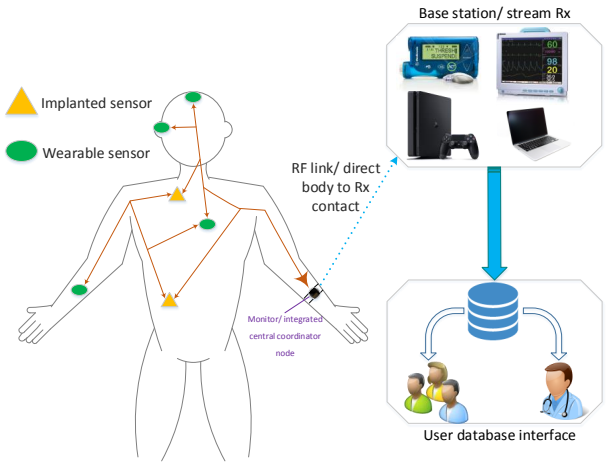

Figure 1.2: Visualized bidirectional IBC links between implanted and on-body sensors transmitting to a central coordinator node for data processing to be viewed directly by a wearable integrated monitor or sent to a base station (which include continuous glucose monitor[7], ECG[8] and PS4[9]) and finally transmitted to a data base for the purpose of long-term storage.

an integrated wearable monitor that observes the vital signs statistics, such as heart pules or glucose level, or to be wirelessly transmitted to a base station. The base station offers more computation power which leads to higher processing and data storage capability. A RF standard with high bandwidth, such as WLAN, can be used by the wearable integrated transmitter for base station-central node transmission. Finally, the processed data of the base station could be sent to a database for long-term storage. The database eases medical personal data access for any authorized user or doctor which can be critical in an emergency situation.

The basic components of this approach include transmitting couplers that induce in-body signal to propagate through the body and to be acquired by the receiving detectors. The couplers and detectors are located in direct contact or in close proximity to the human body. Two main principles of IBC have been investigated to accomplish intra-body transmission which include galvanic coupling and capacitive coupling. Along both techniques, transmitting coupling electrodes and receiving electrodes are required to perform IBC; However,

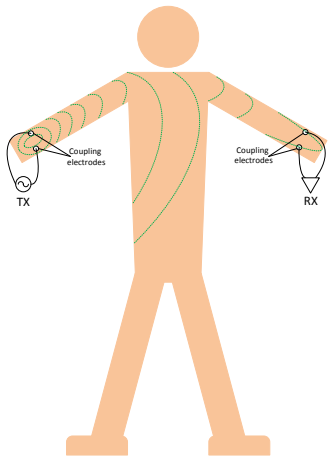

Figure 1.3: Galvanic coupling IBC technique.

direct electrode-skin contact is necessary to achieve galvanic coupling which is the opposite setup in case of capacitive coupling. More details are in the following two subsections.

1.2.1 Galvanic Coupling Approach

This coupling technique is the main focus of this thesis for different factors that are explained in subsequent sections. In this approach, both transmitting electrodes are placed directly on the human skin and very small alternating current is injected using these terminals. While a large portion of the injected current is mutually co-located between the transmitting electrodes, a small traveling current initiates body confined electromagnetic propagation that results in potential difference between receiving electrodes, as shown in figure 1.3. The observed flowing current implies that the human body acts as a transmission line that is affected by the intrinsic dielectric properties.

1.2.2 Capacitive Coupling Approach

Capacitive or electrostatic coupling is another common technique of IBC systems. In this topology, the exciting and receiving electrodes are attached to the human skin while the

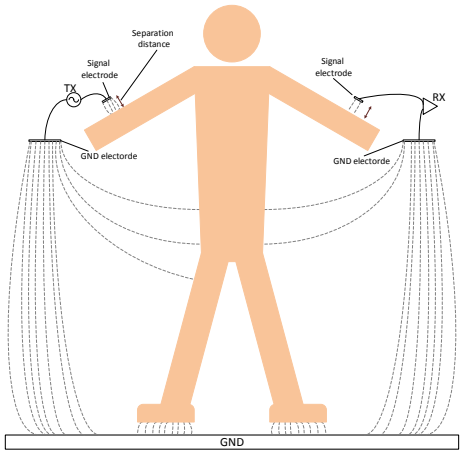

Figure 1.4: Capacitive coupling IBC technique.

reference electrodes (GND) of Tx and Rx are left exposed to the air to form a capacitive return path, as shown in figure 1.4. The transmitting and receiving signal electrode can be placed directly on the human body or relocated to be in close proximity to the body. The Tx signal electrode initiates an electric field to the human body which results in body potential that is different from the environment due to body electrostatic charging. Moreover, the charged body imposes mutual body-environment electric field and induces electric field between the body and the Rx signal electrode which eventually forms a current loop between the body and through the environment ground. The main disadvantage of this setup is that it can be impacted by the surrounding medium in the form of interference.

1.2.3 Comparison of Coupling Approaches

Conducting a comparison and weighting the cons and pros of both coupling techniques is important to determine which of these approaches is more suitable to meet the WBAN requirements and overcome the standard wireless technologies limitations.

In terms of system setup, the galvanic method requires both pairs of Tx and Rx electrodes to be in direct contact to the human body, in contrast the capacitive Tx and Rx signal electrodes has to be in close proximity or in direct contact to the body. Also, the capacitive technique requires an unattached ground electrode to serve as a reference to the environment ground, while this is not part of the galvanic coupling topology which does not need the ground electrodes as a reference.

The technical properties of the galvanic approach entail controlling the induced signal by varying the amplitude of the injected alternating current; Meanwhile, manipulating the induced signal for the capacitive method is achieved by varying the applied electrical potential. Moreover, the established current loop in the capacitive technique is influenced by the environment and surrounding devices that may couple to the transceiver system resulting in interference; However, since the body acts as a waveguide in the galvanic coupling approach, the transceiver is robust against the surrounding electrostatic and electromagnetic radiations. Finally, the position of the subject, such as sitting or standing, may affect the signal quality in the capacitive method since the distance between the electrode and environment grounds is varying by changing the position of the subject[19]; On the other hand, the lack of reference ground in galvanic technique provides position freedom since it does not affect the signal quality. Table1.3 summarizes the difference between both coupling topologies which shows the points of strengths and weaknesses between both methods.

The presented pros and the lack of research focus from the engineers community for the galvanic coupling approach encourage choosing this topology as the superior candidate over

Table 1.3: Summary of comparison between galvanic coupling and capacitive coupling.

Galvanic Coupling	**Capacitive Coupling**
Electrodes have to be in direct contact to the body	Electrodes can be close to or in direct contact to the body
Ground electrode is not needed as a reference	Ground electrode must be included as a reference
Amplitude of the injected alternating current controls the intensity of induced signal	Electrical potential difference controls the intensity of induced signal
Robust against interference from environmental and surrounding radiations	Susceptible to interference from environment and surrounding radiations
Lower transmission data rate [19]	Higher transmission data rate
Position of the subject does not influence the transmission gain profile	Position of the subject may influence the transmission gain profile

the capacitive method for this thesis.

1.3 Thesis outline

Chapter 2 summarizes some of the most significant contributions of IBC research including research papers, journals and dissertations to have a better background about IBC field and to avoid working on some points that were already introduced and solved.

Chapter 3 includes theoretical and finite element method simulations in order to investigate and collect gain profiles of the human channel with considerations of different factors and inputs that may influence the performance of the channel.

Chapter 4 introduces human phantoms and studies several phantom preparation techniques including their experimental setup and final measurements values with a novel approach of making a phantom for each tissue of the human arm.

Chapter 2

General Literature Review

2.1 Introduction

In order to solve IBC system's shortcomings and avoid focusing on already researched theories and techniques, an IBC literature review is required. This section presents a summary of some significant research papers and dissertations that investigate IBC as a transmission alternative.

2.2 Zimmerman, Thesis, 1995

In 1995, the first successful Intra-body communication system was introduced by Zimmerman [17]. The interest emerged out of a research conducted by MIT Media lab on using electric field sensing to determine object's position. Consequently, the motivation to interconnect wearable and carry-on devices with low powered, cheaper and smaller in size system hardware drove the author to investigate the validity of electrostatic coupling to transfer information which is known as capacitive coupling.

By calculating the internal resistance of the human body and comparing electrode to body impedances, the human body is approximated as a perfect conductor. To derive a human channel model, all electric fields that result from electrostatic coupling are identified. Every capacitive coupling is calculated as pure reactive impedance to define the lumped-circuit electrical model. A coil is connected in parallel with the body to determine body to environment capacitance by measuring the resonance frequency. A lock-in amplifier is utilized to measure electrode capacitance.

The coupling electrodes' size and shape is defined by the chosen wearable or portable object; For example, wrist watch, shoes and credit cards. The hardware components of suggested system consist of analog circuitry controlled by micro-controller with all components implemented on a single CMOS integrated circuit. Half-duplex transceiver is preferred over full-duplex transceiver in order to avoid receiver electrostatic field saturation. On-off keying (OOK) and direct sequence spread spectrum (DSSP) modulation techniques are investigated on the same implemented hardware system. Although DSSP reported higher received signal, OOK was the optimal modulation method due to the complexity of phase detection in the case of DSSP. The suggested PAN system showed a bit rate of 2400 bit per second.

2.3 Handa et al., Paper, 1997

The main objective of this paper is to investigate the transmission gain of very low-power health monitoring systems by attaching both transmitting and receiving electrodes and coupling the required signal directly into the human body which is known as galvanic coupling [20]. The bio-signal of interest was an ECG signal which is detected by the ECG detector. Pulse-width modulator with a sampling frequency of 900Hz and carrier frequency of 70KHz is utilized by the detector to couple the modulated signal with power of 8μW to the relay transmitter.

The transmitted signal through the body is detected by the micro data recorder or relay transmitter initially by amplifying the signal, filtering and demodulating it. Finally, prior stage is followed by FM modulation for wireless radio wave propagation. The final result of transmission system shows the detected ECG without any significant distortion which is very promising to pursuit for further research in this coupling approach.

2.4 Lindsey et al., Journal, 1998

The proposed transceiver system includes a function generator with a fixed voltage of 3.25V rms, a current limiting resistor to vary the value of input current into 1mA,2mA,3mA rms and couple it galvanically, Ag-AgCl electrodes, EMG amplifier and oscilloscope. All measurements has been conducted on a cadaver tissue [21].

The transmission results shown by the oscilloscope prove that injected current is proportional to transmission gain as well to the inter-electrodes separation. However, transceiver electrodes separation distance and signal frequency is inversely proportional to the transmission gain.

2.5 Partridge et al., Paper, 2001

Upon the transceiver system presented by Zimmerman, FSK modulation is used to replace OOK modulation technique in order to increase the overall performance of the physical and encoding layers [22]. The carrier frequency was set to 180kHz and 140kHz to ensure avoiding the body antenna effect. The transmitting voltage of 20V was selected.

The transmitting electrodes and circuit were placed on a cardboard box which represents a wearable device with capacitive coupling electrodes. When the subject touches one of these

electrodes, a return path is formed between the grounding environment and to one of the receiving electrodes that are attached to the subject. Different electrodes positioning has been investigated which showed that shoe position recorded the highest signal strength. The transceiver system implemented a data rate of 38.4kbps.

2.6 Oberle, Dissertation, 2002

The galvanic coupling approach has been chosen to implement a low-power biomedical communication system [23]. A simplified engineering model has been derived with respect to the human tissue's dielectric characteristics. The coupled alternating current is in the range of μA. The transceiver communication system utilized continuous phase frequency shift keying (CPFSK) modulation with encoding frequencies of 51.2kHz and 61.4kHz which provided a data rate of 4.8kbps.

2.7 Fujii et al., Paper, 2003- 2006

The main focus of this work is to capture the influence of transmitter ground electrode on surrounding and penetrating electric field which is the result of electrodes capacitive coupling [24]. The transmitter components which includes electrodes and circuit board are modeled as perfect conductor sheets to simplify power calculations after deriving the circuit model and to enable the use of FDTD calculations.

The human arm model has been selected and modeled as a rectangular parallelepiped with dielectric properties of muscle tissue. For simpler equivalent circuit derivation, common transmission line laws are imported.

A sine wave with 3V amplitude and 10MHz frequency is fed to the transmitting electrode.

With both GND configurations, attached and not attached transmitting electrode ground, the first setup showed full electric field distribution along the arm due to electric field penetrating the arm. On the other hand, the lateral configuration showed an electric field with less intensity resulting from the increase in reactive value of the human input impedance.

2.8 Hachisuka et al., Paper, 2003- 2005

By using a function generator which is connected to Ag-AgCl electrodes that are attached to a human arm and an oscilloscope to detect the galvanically coupled signal, the authors were able to determine the basic transmission characteristics of the human body [25]. The transmission results confirm that the frequency of 10MHz has the highest transmission gain.

To determine the electrode's contact impedance, the simple circuit model was applied. It had been shown that regardless of the electrode metal material, the obtained impedance had small value fluctuation.

Moreover, a phantom solution has been fabricated to replace the need for biosignal experimentation which provided nearly the same gain as in human measurements at 10MHz. By using FM and FSK modulations, the authors observed a robust human channel communication against surrounding noisy devices with data rate of 9600bps.
Further research by the authors proved that two-electrode arrangement or electrostatic coupling is superior to the galvanic coupling [26].

2.9 Shinagawa et al., Journal, 2003- 2004

The main contribution of this work is to replace the common signal detection technique that utilizes a regular oscilloscope probe with an electrooptic (EO) probe [27]. The electrooptic

sensor consists of both transverse and longitudinal type for sensing all electric field orientations. In addition, this sensor offers low electric field intensity detection due to the very high input impedance and ultrawide detection band.

Two personal digital assistants (PDA) are connected to the transceiver system to transmit an information and verify receiving it correctly. All components are battery powered and suspended in the air to mimic an actual transmitting situation. A coupling voltage of 25V is assigned to the transmitting circuit; However, less than 100mV is induced on the human body.

Finally, by sending a connection confirmation command, the authors confirmed a half-duplex communication in accordance with IEEE 802.3 with data rate of 10Mbps.

2.10 Wegmueller et al., Journal, 2005- 2010

The galvanic coupling approach had been investigated thoroughly in this work [28]. The finite element method (FEM) alongside with *in vivo* measurements from 20 subjects has been conducted to estimate the human channel attenuation. A meshed cylindrical object which mimic the geometry and tissue thicknesses of the human arm, which has the same geometries of the imported cylinder that is going to be explained in detail in the coming chapters, has been imported to the ANSYS-EMAG package.

The presented final results of FEM and experimental measurements demonstrate gain value agreement at various frequencies that evaluate the effect of electrodes' size of both TR and electrodes transmission distance. The size of transmitting electrodes is proportional to the coupling gain. On the other hand, the muscle tissue resistivity and electrodes distance is inversely proportional to the gain. Different electrodes placing on the thorax area yields location independent gain data with channel capacity of 130kbps and 30kHz channel band-

width.

Further conducted research by the group implemented an enhanced system components which improved the thorax channel capacity to 0.87Mbps [29]. Nevertheless, higher data rate of 1.23Mbps is observed along the upper arm channel. The influence of different prefabricated electrodes has been tested which resulted in gain dependent data.

2.11 Ruiz et al., Papers, 2006- 2007

A transmission frequency range between 1MHz-2.5GHz has been investigated by the authors in terms of received signal power magnitude [30]. In addition to setting an environmental ground, a signal electrode is isolated vertically from a reference electrode (GND) which is connected to the ground of a network analyzer for both TX and RX electrodes where two setups of GND electrode touching the skin or not touching it are included . The network analyzer is used to display the received signal. The acquired data from the network analyzer verify that as the distance of transmission and the signal frequency increase, the detected signal magnitude decreases.

A signal generator that is able to generate and modulate a radio signal in order to propagate it thorough the human body and a wireless communication analyzer that is capable to detect, demodulate and plot the received signal are implemented to evaluate the performance of digital modulation technique using intra-body channels. MSK, BPSK, QPSK, 8PSK and 16QAM were the digital modulation schemes of transmission with symbol rate of 100ksps to 5Msps. By contacting the signal electrode to the human body, which is referred by the authors as intra-body channel, along the five modulation methods showed superior performance comparing to the other setup, which is referred to as air propagation, where MSK modulation reported the best performance, but 16QAM the farthest symbols to the

reference constellation points of the constellation diagram when the symbol rate is 100ksps and transmission distance is 60cm. By increasing the transmission distance and symbol rate, BPSK provided the best performance.

By using Error vector magnitude (EVM), the authors were able to quantify the difference between the ideal and measured signal. The EVM measurements provided that BPSK modulation with symbol rate of 2.5Msps could be used for transmission distance below 155cm to achieve high detection accuracy and good modulation quality. Also, it provided 5Msps for distance of 20cm for BPSK and MSK modulations.

More research by the authors aimed to derive a statistical channel model of intra-body propagation characteristics relying on the best fitting probability function where multiple families of probability distribution such as T-location scale, extreme value, normal, logistic and non-parametric are chosen based on their shape [31]. The same experimental setup had been applied on this paper; However, walking and static body situation has been tested to investigate its effect on human channel performance. The normal distribution showed the best fitting along all specified electrodes' placement. Finally, the authors were able to define a general linear statistical model for a reasonable range of transceiver distance.

2.12 Journals, 2010- 2016

Yong Song and other co-authors had derived a transfer function that is able to capture the geometrical and dielectric properties of the human channels [1]. The proposed transfer function and distributed impedances has been imported to this thesis for further investigations which is going to be explained in detail in the coming chapter. All the human parts had been simplified into multiple concentric cylinders to construct a circuit model where each cylinder represent a human tissue with permittivity and conductivity values imported from Gabriely

et al. and a diameter of 50mm is assigned to the largest cylinder of the arm with specific diameter for each tissue and set in proportion for other human parts. The measurement and simulation attenuation profiles of all presented human channels showed data agreement with a constant error which had been neutralized using a correction factor defined as K.

A comprehensive experimental measurement for both coupling approaches was presented by Callejon et al. to explore a suitable operating frequency range and to determine the influence of electrodes' types, channel length and grounding strategy [19]. The experimental setup of galvanic coupling included a signal generator, oscilloscope, coupling electrodes and baluns to eliminate the effect of internal ground of signal source and detector. A spectrum analyzer has been used in the capacitive setup to transmit and detect the coupled signal where the rest of experiment components are the same as the galvanic setup. Over a 100 experimental measurements have been conducted. An optimum operating frequency range between 20-60kHz has been determined for the galvanic method and between 60-70MHz for the capacitive approach where the measurements were performed over several days. In addition, the authors affirmed that the material of the electrodes did not have a significant influence on the channel performance; However, the capacitive approach measurements showed sensitivity to grounding electrode type. Also, they confirmed that as the inter-electrode spacing of TX and RX increases, the transmission gain enhances for the galvanic status. Moreover, in case of female subject, the transmission profile showed higher attenuation than the case of male subject since the arm of male has bigger diameter where all the electrodes were placed on the arm of the subject; Nevertheless, the return or flowing path of the capacitive method were not influenced.

Swaminathan et al derived a tissue equivalent model with the same impedances distribution as shown by [1]; In addition, the authors considered the impedance of the path between each human tissue[32]. Finite element method has been utilized to verify the equivalent model which indicated data agreement for multiple transmission paths that are represented

in terms of wearable to wearable, wearable to implant and implant to implant. The muscle to muscle path showed the highest SNR and stable readings compared to the other paths. Transceiver and inter-electrode separation have been investigated which support the results of all prior mentioned authors in this chapter. Finally, experimental measurement has been conducted on a porcine meat to validate the readings of the equivalent model which showed a small readings variation.

2.13 Conclusion

This section summarized the main contributions and results of several significant research papers and dissertations that investigate intra-body communication as a transmission technique. However, different approaches have been conducted to study this technique. In addition, these approaches vary even for the same coupling method. For example, research presented in [25][32][1] is based on deriving a transfer function in order to obtain a gain profile and validate *in vivo* measurements; On the other hand, the approach shown in [31] relies on deriving a statistical model that is able to evaluate and predict the behavior of IBC system. Table 2.1 shows a summary with crucial details of each selected research paper and thesis of IBC method.

All of the presented research in this section did not reach a consensus on the optimum operating frequency of IBC. Hence, different frequency ranges are chosen for each coupling method. Nevertheless, all of the selected frequency ranges for the galvanic approach, which is the interest of this research, are in the ranges of KHz, e.g. [32][20][21], or below 10 MHz, e.g. [28]. Investigating a wider frequency range within higher frequencies may prove to determine higher optimum frequency which results in employing a higher transmission rate.

The setup and location of electrodes is investigated in reviewed papers. The authors in

Table 2.1: Summary of reviewed IBC systems properties.

	Coupling	V/A	Freq.Range	Tx/Rx Separation	Electrode Size	Modulation	Data Rate
Zimmerman	Capacitive	30V	100-500kHz	Wrist watch to wrist watch	25x25,30x30, 70x20,80x80, 130x40, 900x25mm^2	OOK	2.4kbps
Handa	Galvanic	20μA	10-100kHz	Chest to wrist	-	PWM	0.9kbps
Lindsey	Galvanic	3mA	2-160kHz	10, 20cm	13.14πmm^2	FM	-
Partridge	Capacitive	22V	140-180kHz	Hand to(watch,belt,shoe)	15x15,30x14, 100x100,250x250cm^2	FSK	38.4kbps
Oberle	Galvanic	4mA	-	-	-	CPFSK	4.8kbps
Fuji	Capacitive	3V	10-100MHz	-	2x3,1x3,0.5x3cm^2	OOK	9.6kbps
Hachisuka	Capacitive	1V	10k-50GHz	28cm, 50-300mm	30x30,20x20mm^2	FSK	9.6kbps
Shinagawa	Capacitive	25V	-	1m	-	-	10Mbps
Wegmueller	Galvanic	1mA	10k-1MHz 1k-10MHz	Two locations on (upper arm,thorax)	880mm^2, 54, 560cm^2	FSK,BPSK	128, 255kbps
Ruiz	Capacitive	-	200-600MHz	90, 155cm	π/4,π, 2.25πcm^2	BPSK,MSK	100-2500kbps
Song	Galvanic	5V	100k-5MHz	20, 30, 40cm	25πmm^2	-	-
Callejon	Gal/Cap	5V	10k-2MHz 1M-100MHz	Multiple locations (arms,torso,legs,back)	π/4, 2x2 3x3,4x4,7x7cm^2	-	-
Swaminathan	Galvanic	1mA	100k-1MHz	0.2-40cm	10x10mm	-	-

[28][1][21][19] showed the influence of transmission distance that separates the electrodes wherein the last two examined the inter-electrodes spacing effect of transmission. However, only the author in [32] reviewed the effect of changing the inter-electrode spacing of only the receiving electrodes. Thus, thorough study on inter-electrode spacing effect is needed.

The most frequent chosen medium for authors, which is the most reliable one, to validate simulation results of IBC is the human body as shown in [22][28][30][1][19]. However, to guarantee the safety of participants, other transmission mediums with similar properties are preferred. The research in [21] shows the use of a cadaver to conduct measurements which is very difficult to find. The authors in [27][25] followed simpler approach by using a polymeric material and polyvinyl chloride, respectively. The author in [32] utilized porcine tissue to conduct the experimental measurements. These non-human mediums may have similar properties to human body; However, a phantom that mimics the properties of each tissue in the human body can improve the accuracy of experimental measurements.

Chapter 3

Human Channel Modeling

3.1 Introduction

Intra-body communication method which is achieved using capacitive or galvanic coupling requires several approaches to investigate its validity and to gather signal transmission data along the human body for this technique. The most suitable initial approach is to create a model that is able to predict the quality and intensity of the output signal given a certain input signal.

Human channel modeling can provide an estimation of the transmission attenuation profile with approximated collected data. Since this approach produces relative gain values, data variance to conducted experimental measurements exist. The first step of human channel modeling is by innovating a human tissue parametric model for the purpose of developing an analytical equivalent circuit model. Other channel modeling techniques include performing finite element method (FEM) on constructed designs that mimic the geometry and internal characteristics of the human body tissues. The modeling of the human channel must take in consideration and capture the following characteristics:

- The influence of the external and internal tissues properties (including skin, fat, muscle and bone) on the transmission quality.
- The geometry and dimensions of the chosen body channel.
- The coupling and detecting electrodes dimensions, separation distances and material, if effect of material is detected.
- The thickness of human channel tissues and the role it plays on transmission gain values.
- Which of the tissues facilitate current path along the human channel.

By addressing these points, the resulting human channel model can produce an accurate transmission data with minimal error, yet averaged and approximated input values are used to simplify calculations.

This chapter starts by introducing the human tissue parametric model, then equivalent circuit model and ends with finite element method simulations of IBC.

3.2 Parametric Model of the Human Tissue

For the purpose of comprehending the propagated signal behavior and paths along the human channel, the human tissue dielectric properties have to be defined. By conducting empirical measurements and deriving equivalent models, researchers were able to capture the human layered tissues characteristics and dielectric values.

The dielectric properties of human tissues can be characterized in terms of permittivity ϵ_r and conductivity σ. The permittivity of a tissue is its resistivity to form an electric field through the tissue, in other words, its ability to store a unit charge under the influence of

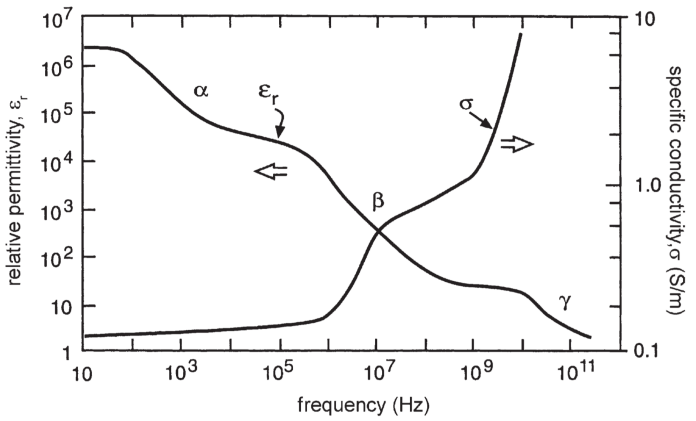

Figure 3.1: Human tissues variations of relative permittivity and conductivity values which show the three main dispersion regions [10].

an electric field. On the other hand, the conductivity of the tissue is its ability to transport charge. Due to the heterogeneous property of the human tissue, both values of ϵ_r and σ of the tissue are frequency dependent. This alteration of dielectric properties with respect to the operating frequency is characterized in terms of dispersion regions.

Relaxation Regions Characterization

The charge carriers' behavior and tissue dipoles orientation define the relaxation or dispersion regions. At low frequency range, such as below 1kHz, alternating applied external field imposes tissue dipoles orientation response and longer distances of transportation for the charge carries. In contrast, as the frequency increases to high ranges, the polarization effect discontinues which results from less dipoles orientation change with respect to the applied field. The dispersion frequency can be defined in terms of angular relaxation frequency ω_r or relaxation time T_r where

$$\omega_r = 2\pi f_r,\ T_r = \frac{1}{f_r} \tag{3.1}$$

The dispersion regions are characterized in terms of (α), (β) and (γ) relaxation regions as

shown in figure 3.1. The (α) dispersion exhibit ions transportation across a biological cellular membrane at frequencies ranging between 1Hz and 100kHz, whereas high permittivity and low conductivity values is evident. As the frequency increases to the MHz range, tissue cellular membranes polarization starts to act as a barrier to the flow on ions between the intra- and extra-cellular content. In addition, protein polarization contributes to the second main dispersion so-called (β) relaxation. Finally, in the GHz frequency range, water molecules polarization causes the (γ) dispersion where the permittivity values of human tissues are at minimal.

Tissues Modeling Techniques

The three distinctive dispersion regions define dielectric properties variation for the human tissue which facilitate deriving a proper parametric model. The Cole-Cole equation [33] introduces the frequency-dependent dielectric values alterations that results from polarization characteristics with

$$\epsilon^*(\omega) = \epsilon_\infty + \frac{\Delta\epsilon_n}{1 + (j\omega\tau_n)^{(1-\alpha_n)}} \tag{3.2}$$

where ϵ^* is the complex dielectric constant, ϵ_∞ is the permittivity at infinite frequency, $\Delta\epsilon_n$ is the magnitude of dispersion calculated by $\Delta\epsilon_n = \epsilon_s - \epsilon_\infty$ in which ϵ_s is the permittivity at static frequency. ω is the angular frequency, τ_n is the relaxation time constant in which the period extension of this constant indicates molecular dipoles orientation response at short periods and ions flow at long periods. The distribution parameter α_n ranges between 0 and 1 which is correlated to the main dispersion regions broadening. In contrast, the decrease of these regions can be defined in terms of multiple Cole-Cole equations summations for the

complex permittivity equation as in the following

$$\epsilon^*(\omega) = \epsilon_\infty + \sum_n \frac{\Delta\epsilon_n}{1 + (j\omega\tau_n)^{(1-\alpha_n)}} + \frac{\sigma_i}{j\omega\epsilon_o} \tag{3.3}$$

where σ_i is the static ionic conductivity. What distinguish Cole-Cole equation summation, described in (3.3), from other derivations such as Havrilak-Negami and Cole-Davidson equations is that it can be applied specifically to the biological materials like the layered human tissues to conduct dielectric properties calculations [34]. In addition to the frequency dependent permittivity, equation 3.3 can be used to derive the complex conductivity of each tissue with respect to the frequency using

$$\frac{[\epsilon_s - \epsilon_\infty].\epsilon_o}{\tau} = \sigma_\infty - \sigma_s \tag{3.4}$$

where σ_∞ and $\sigma_s$is the conductivity at infinite and static frequency,respectively. By using equation 3.4, the complex conductivity σ^* and the complex impedance z^* of each tissue are

$$\sigma^* = j\omega\epsilon_o\epsilon^* = \sigma_\infty + \omega\epsilon_o\epsilon_\infty \frac{[\epsilon_s - \epsilon_\infty]}{1 + j\omega\tau},\ z^* = \frac{1}{\sigma^*} \tag{3.5}$$

The Cole-Cole equation which is described in (3.3) can be represented in terms of an RC (resistive, capacitive) equivalent circuit model. By setting the distribution parameter $\alpha_n = 0$ with a single time constant, an ideal capacitor, a resistor and a constant phase element (CPE) are connected in parallel to establish the circuit model as shown in figure 3.2. The CPE part includes a series combination of a complex valued impedance components given by the following

$$Z_{CPE} = A(j\omega)^{-n} \tag{3.6}$$

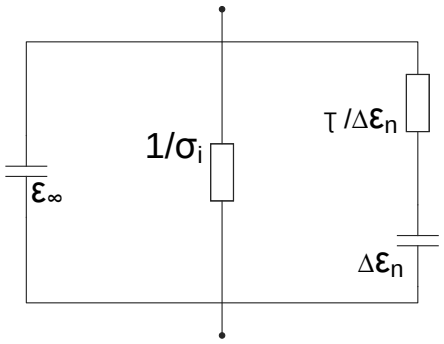

Figure 3.2: The equivalent circuit model of Cole-Cole equation with α_n=0 and a single time constant.

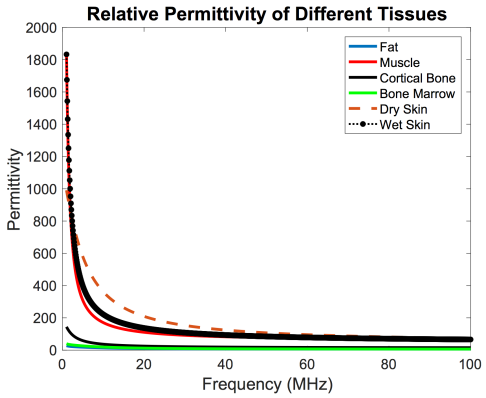

Figure 3.3: The frequency-dependent relative permittivity measurements and calculations of the human layers tissues including bone marrow, cortical bone, muscle, fat, skin (wet and dry conditions) tissues.

Where A is a constant and n=α_n. The value of n determines the value of Z_{CPE} whether it is pure resistive, n=0, or pure reactive, n=1.

The most profound utilization of equations [3.3, 3.5] to calculate the complex permittivity and conductivity of each human tissue was achieved by Gabriel et al [35]. The empirical measurements and calculations were conducted on bone marrow, cortical bone, muscle, fat and skin tissues with a selected frequency range of 10Hz-20GHz; However, our frequency range of interest for this thesis is determined between 1MHz-100MHz as shown in figure 3.3 and figure 3.4. The skin condition alters its dielectric properties, hence wet and dry conditions of the skin is taken in consideration. The high values of relative permittivity and conductivity of muscle tissue compared to the other four tissues suggest a dominant influence

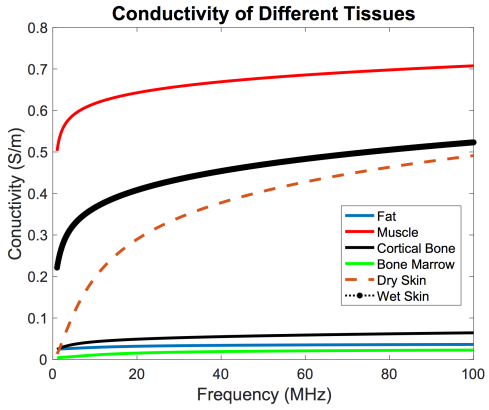

Figure 3.4: The frequency-dependent conductivity measurements and calculations of the human layers tissues including bone marrow, cortical bone, muscle, fat, skin (wet and dry conditions) tissues.

on the signal transmission by the muscle tissue.

3.3 Equivalent Circuit Model of Human Channel [1]

3.3.1 General Model of the Human Channel

To verify the legitimacy of galvanic IBC coupling, an analytical equivalent circuit model (AECM) is adopted in this thesis to obtain the coupled signal transmission gain profile [1]. The starting point to initiate an AECM is by deriving a transfer function that is able to capture the internal and external geometrical and electrical properties of the chosen body limb or organ. Moreover, the coupling electrodes' size, the contact distance between skin and electrodes, the spacing between the electrodes of the transceiver and the inter-electrode spacing of the transmitting and receiving electrodes must be included within the transfer function calculations. By importing the derived transfer function H_A, the attenuation profile

[1] The formulas and models presented in this section are imported from [1].

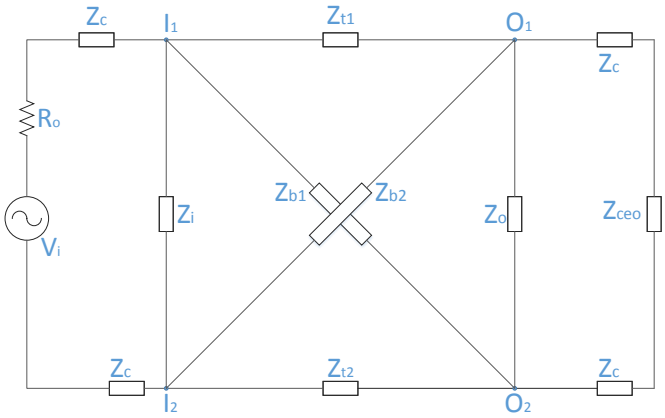

Figure 3.5: Equivalent circuit model for galvanic coupling which includes V_i as the transmitter voltage, R_o and Z_{ceo} are the transmitter output resistor and receiver input impedance respectively, Z_c is the coupling impedance , Z_i is the input impedance , Z_o is the output impedance, Z_{b1} and Z_{b2} are the cross impedances . Z_{t1} and Z_{t2} are the transmission path transverse impedances.

is as follows

$$G = 20 \log_{10} H_A + K \tag{3.7}$$

where K is the correction factor that enables to modify the uniform error within defined gain values.

As shown in figure 3.5, the proposed model of the galvanic coupling represents a four-terminal circuit where V_i is the transmitter output voltage, R_o and Z_{ceo} are the transmitter output resistor and receiver input impedance respectively, Z_c is the coupling impedance between the human skin and the transmitting or receiving electrodes, Z_i representing the input impedance between the two input terminals I_1 and I_2 which channels the majority of the current between the two terminal, Z_o is the output impedance between the two output terminals O_1 and O_2 which channels the lesser portion of induced current between the two terminals , Z_{b1} is the cross impedance between I_1 and O_2, Z_{b2} is the cross impedance between I_2 and O_1. Z_{t1} and Z_{t2} are the transmission path transverse impedances.

The intrinsic value of this AECM is to acquire a general transmission gain values with respect to operating frequency of coupled signal along the human channel, hence determining the optimum signal frequency. However, more detailed results of AECM can be obtained by including the five layered tissues into transfer function calculations.

3.3.2 Layered Tissues Model of the Human Channel

The complexity of the human body which includes organs and glands with different major functions leads to difficult human channel path loss estimation. By choosing a specific human channel that does not include complex organs, it results in easier equivalent circuit model derivation. The human arm is the prime candidate to obtain the path loss of the human channel due to its less complex internal content which includes the previously mentioned five main tissue layers and the practical future use of placing sensors or devices on the human arm with data transmitting or receiving functions.

The derived AECM for galvanic coupling can be implemented along the five stacked tissues to obtain the estimated gain profile of coupled signal with higher accuracy as shown in figure 3.6. Each of the presented impedances is characterized for every tissue to include its dielectric properties in AECM calculations. Every impedance, except the coupling impedance Z_c, is denoted with two subscripts, generally $Z_{(q)(u)}$ where the q indicates the tissue layer, e.g. "$_s$" for skin, and the second index denotes the type of the impedance, such as "$_t$" for transverse impedance. These impedances form multiple current path flows with a dependent current value on tissue's electrical properties.

The skin tissue plays a major rule on transmitting the coupled signal because of its direct contact with transmitting and receiving electrodes and due to the good conducting property. The poor conductivity of fat tissue drives this layer to act as a barrier between the skin and muscle. However, the large exchanged current between the two terminals of the transmitting

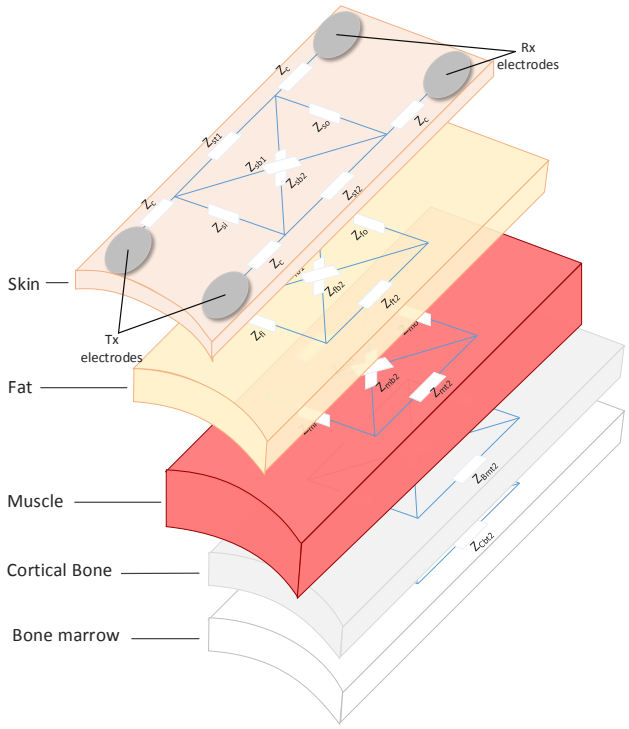

Figure 3.6: Equivalent circuit model of layered tissues for galvanic coupling.

electrodes can penetrate the fat tissue portion located under these electrodes and induce flowing current within the muscle tissue. Due to the higher conductivity of muscle tissue comparing to the remaining tissues, more ions are flowing to the muscle tissue portion that is located under the receiving electrodes which result in potential difference within these detecting electrodes.

The parallel connection of the derived impedances of the layered model capture the geometrical and dielectric properties of each arm tissue. According to AECM, the modeled impedance between the two terminals of transmitting and receiving electrodes is the input Z_i and out impedances Z_o, respectively. This impedance for a specific tissue is mainly affected by the thickness of the determined layered, the geometrical and dielectric properties

of the human tissues. The formula of Z_i and Z_o is defined as in the following

$$\begin{aligned} Z_i = Z_o =& \frac{1}{\sum_{n=1}^{5}(\frac{\sigma_{nf} S_n}{L_q} + j\omega \frac{\epsilon_{rnf}\epsilon_o S_n}{L_q})} \\ =& \sum_{n=1}^{5} \frac{L_q}{\sigma_{nf}\pi r^2 + j\omega\epsilon_{rnf}\epsilon_o \pi r^2} \end{aligned} \tag{3.8}$$

Where L_q is the thickness of the related tissue, σ_{nf} and ϵ_{rnf} are the conductivity and relative permittivity, respectively, corresponding to the n_{th} human body tissue and to the input signal frequency. S_n is the cross-sectional area of the n_{th} layer.

By modeling the transmission path, transverse impedance Z_t is derived. This impedance depends mainly on the distance of transmission between Tx and Rx electrodes. The transverse impedance is defined as follows

$$\begin{aligned} Z_t =& \frac{1}{\sum_{n=1}^{5}(\frac{1}{R_n} + j\omega C_n)} \\ =& \frac{L}{\sum_{n=1}^{5} \sigma_{nf} S_n + j\omega\epsilon_o \sum_{n=1}^{5} \epsilon_{rnf} S_n} \end{aligned} \tag{3.9}$$

where L is the signal transmission distance between the transmitting and receiving terminals. The total transverse impedance along the transmission path corresponding to the tissue layers of the human arm can be calculated by summing all Z_t with respect to every tissue.

The simulation results of AECM with varied transmission distance between the coupling and detecting electrodes are shown in figure 3.7 [36] [2]. It is clear that by increasing the distance of transmission, higher attenuation occurs which is shown as a decrease in transmission gain values. Consequently, It can be seen that an increment of 5cm in transmission distance results in attenuation of $\approx$ 4dB. The transverse impedance Z_t is proportional to the transmission distance. Thus, higher values of Z_t attenuates the coupled signal to be detected by the

[2] The shown results of this simulation is conducted by Ahmed E Khorshid who is the lead researcher of IBC research group.

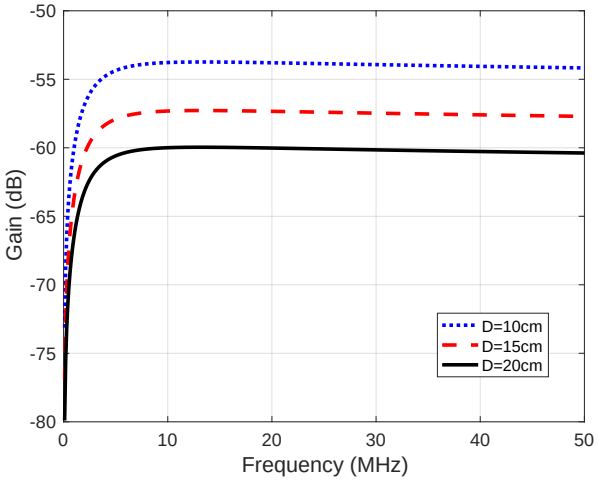

Figure 3.7: Transmission gain in (dB) of the layered equivalent circuit model corresponding to transmission distance altering hence transverse impedance Z_t changing.

receiving electrodes.

With the direct contact of transmitting and receiving electrodes to the human skin, an exclusive impedance to the skin layer labeled as coupling impedance Z_c is derived. Modeling the electrodes of this impedance to theoretical derivation is a complicated obstacle due to the non-fixed characteristics of chosen electrodes that corresponds to the determined electrode type and the existing gap between skin and electrodes. As a result, *in vivo* measurements is preferred to determine the electrodes' characteristic of Z_c . This impedance depends mainly on the size of the attached electrodes, the human skin impedance and the distance of gap between the skin and the electrodes.

The simulation results of the equivalent circuit model with different electrode sizes is shown in figure 3.8 [3]. By increasing the size of the electrodes, the transmission gain values are enhanced. It can be noticed that the optimum transmission gain profile is obtained by setting the size of the electrodes to 6.25 cm^2. Larger electrodes' size result in less transmission attenuation. However, a trade-off between electrode size to ensure user comfort and

[3] The shown results of this simulation is conducted by Ahmed E Khorshid who is the lead researcher of IBC research group.

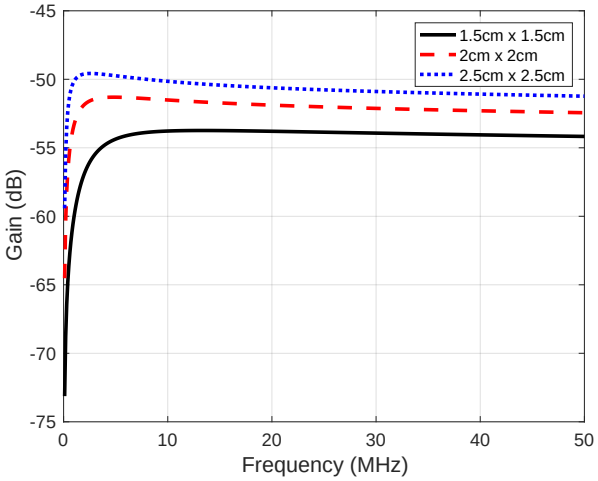

Figure 3.8: Transmission gain in (dB) of the layered equivalent circuit model corresponding to coupling impedance Z_c varying by modifying the size of coupling and receiving electrodes.

transmission gain has to be considered. The impedance of the skin is affected mainly by its condition, e.g. wet or dry skin. Dry skin condition is chosen to determine Z_c of AECM. In our analytical simulation, we assume that the coupling and detecting electrodes are attached perfectly to the skin layer, distance between electrodes and skin= 0 cm, in order to simplify Z_c calculations.

3.4 Finite Element Method Simulation Technique

Fast and safe technique to investigate IBC and to validate AECM results is required. The finite element method (FEM) accomplishes this task by designing a full 3D model that mimic the geometry and content of the human arm and solving the partial differential equations of the simulated applied signal. To achieve FEM, High Frequency Structure Simulator (HFSS) of ANSYS Electronics Desktop was used for accurate full wave electromagnetic simulation to find an estimation of the human channel path loss. The tool can solve Electro-Magnetic (EM) fields for every tetrahedron of the 3D meshed structure of the arm model alongside the transmitting and receiving electrodes.

Implementing FEM using ANSYS is advantageous over AECM due to the following

- FEM utilizes detailed 3D model to conduct signal simulations hence higher gain profile accuracy.
- Easier model optimization and modification as it exploits simple and practical designing tools.
- ANSYS enables visual plot of the current and voltage distribution along the human channel.

The common method to obtain the transmission gain is by determining the values of the applied voltage at the transmitting electrodes (V_i) and initiated voltage at the receiving electrodes (V_o) and finally importing these values into the following

$$G(dB) = 20 \log_{10} \frac{V_i}{V_o} \tag{3.10}$$

However, HFSS enables direct calculations of the transmission gain by determining the scattering parameters or S-parameters of the two applied ports finalized as the coupling and

detecting electrodes. The S_{21} parameter is the targeted parameter to measure the gain of transmission as it defines the voltage gain of terminal 2 , or in this case detecting electrodes' voltage, with respect to terminal 1 voltage which is the voltage of transmitting electrodes.

Detailed Human Arm Model

The full FEM model was based on the model created by NEVA Electromagnetic group which was subsequently imported on ANSYS HFSS environment as shown in figure 3.9.(a)(b) [37]. In addition to the five main layers of human body, blood streams or veins are included in the design of the arm model. Moreover, the detailed geometry of the internal and external structure of the imported model mimics the proportions, dimensions and geometry of an averaged human arm.

Although the detailed model results in higher accuracy, the simulation time is much longer than the required time in case of the concentric cylinders. Furthermore, in addition to the arm, the imported model includes over 25 tissues of other organs and human parts that complicate the meshing procedure of the targeted simulation by adding a high number of meshing elements to the simulation.

Simplified Human Arm Model

A simplified geometry an arm model has also been constructed, as show in figure 3.10. It is completed by building the five main layers that include skin, fat, muscle, bone marrow and cortical bone. The dimensions of the cylinders mimic the average total thickness of the arm related to each tissue thickness [1]. The dielectric properties, which is described in terms of conductivity σ and relative permittivity ϵ, of every tissue are measured and averaged by Gabriel et al [35].

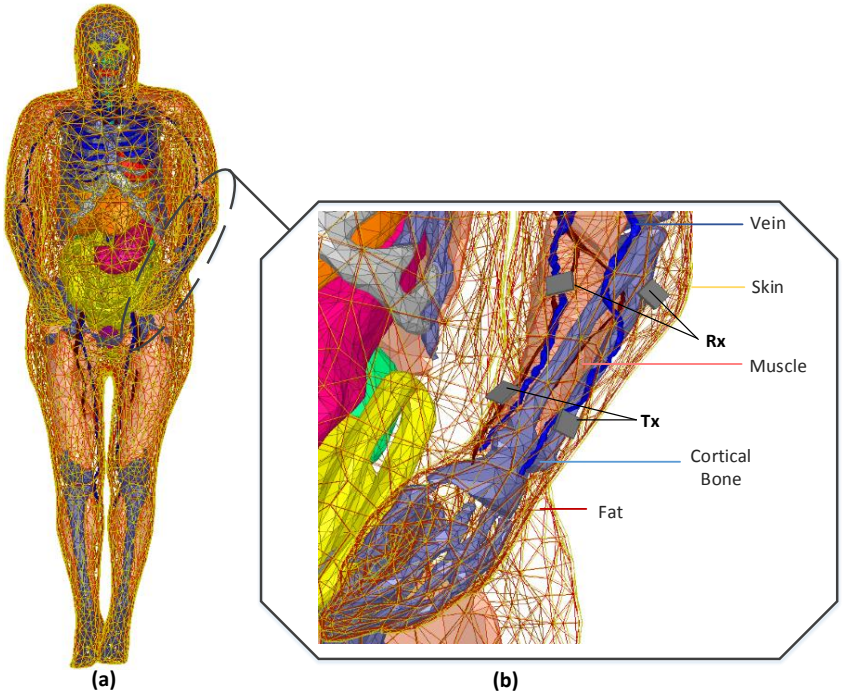

Figure 3.9: The full human model including veins, detailed geometry and content in addition to the five main layers where (a) is the human body and (b) is the human arm in order to conduct FEM simulations.

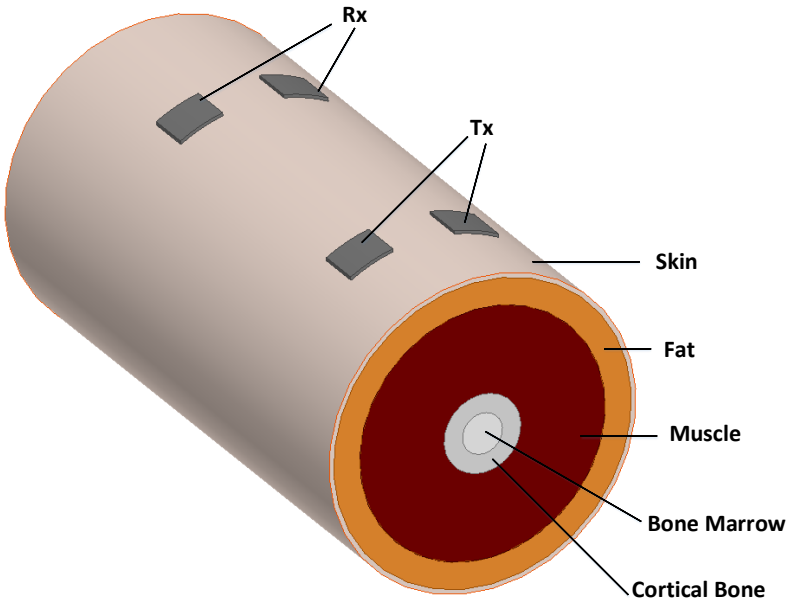

Figure 3.10: Simplified human arm structured by using five concentric cylinders where each cylinder represent an arm tissue for the purpose of conducting FEM simulations.

3.4.1 FEM Simulation Setup

The transmitting and receiving electrode dimensions of both models were 15x15 mm. Since the impedance of the electrodes is independent of the electrode material, Copper is used as the material electrodes [38]. The transmission path length is 10 cm. The excitation of transmitting side is set to a lumped port which allows us to embed internal ports of excitation with an input impedance of 50 Ω. The current source of the exciting ports is set to 1 mA which conforms to the safety standards of the International Commission on non-ionizing radiation protection (ICNIRP) by controlling the power of exciting source [39].

Determining the frequency range of research interest is of high priority as it defines the effect of multiple transmission parameters and the optimum frequencies with least propagation attenuation. In addition, biological properties are factors that has to be considered when choosing coupling frequency, e.g. anisotropy of tissues [34]. The anisotropy characteristic of a tissue illustrates the dependency of tissues' conductivity on orientation or direction of the tissues. This phenomenon is manifest in muscle and bone tissues within low frequencies of propagation . An operating frequency range of 1MHz-50MHz is selected in order to overcome the anisotropy property of biological materials .

3.4.2 Simulation Results

By complying with the simulation setup at previous section, gain profile results of both detailed human arm model and simplified arm model is plotted as shown in figure 3.11. The full-order arm model shows maximum gain of ≈ -54.5 dB at 49 MHz. The concentric cylinders arm model shows an increasing gain proportional to the sweeping frequency, however, both models shows close proximity in gain values.

There are several reasons that contribute to gain readings tolerance between the detailed

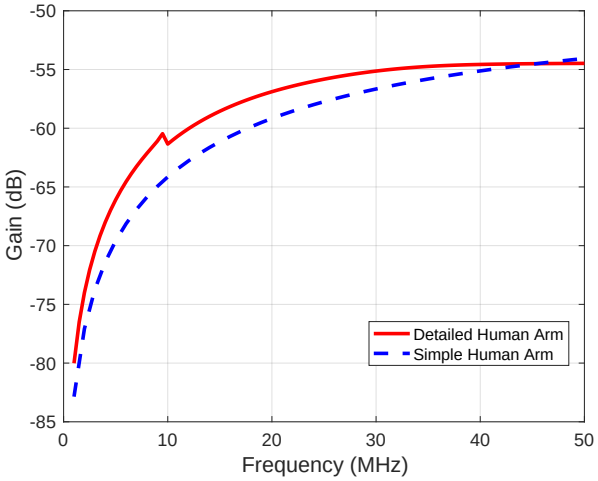

Figure 3.11: Simulation results of transmission gain including the full-order human arm model, solid line, and the concentric cylinders representing the human arm, dashed line.

and simple arm models. The detailed geometry of human arm model which includes veins, uneven thicknesses of muscle and bone layers, the nonuniform surface of skin that affects the positioning of all electrodes structure play a main role in the observed difference of gain values between human and cylindrical model. However, shown results provide that using cylindrical model can be an alternative to using a model with detailed human geometry when targeting less accurate yet fast results of path loss profile. As a result, the cylindrical model is utilized to determine the influence of electrodes' and arm model characteristics in the following subsections.

Impact of Transmission Distance

The influence of separation distance between transmitting and receiving electrodes is achieved by varying D_s which is shown in figure 3.12. It is expected to have higher attenuation values as the transmission distance is increasing since the propagated signal experience more tissue resistance at longer distances and eventually lower detected voltage at receiving terminals.

By changing D_s from 10cm up to 19 cm with a step difference of 3cm, a very small gain

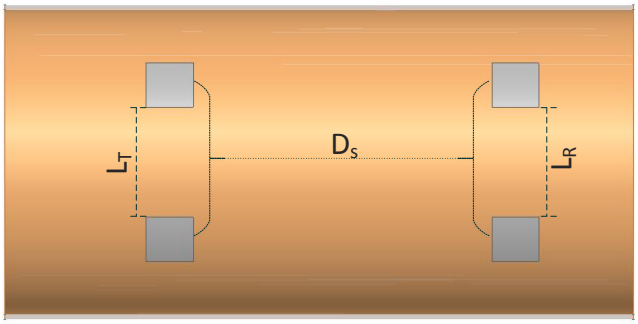

Figure 3.12: Transmission distance D_s separate the Tx and Rx electrodes. L_T and L_R are the inter-electrode spacing between the transmitting and receiving electrodes, respectively.

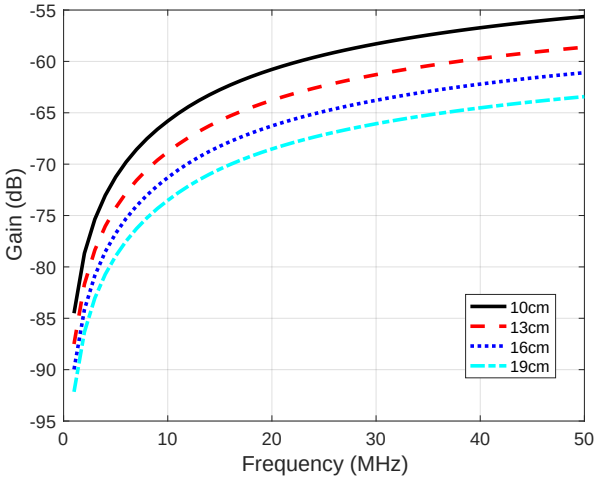

Figure 3.13: Simulation results of IBC signal transmission with respect to varying the separation distance between Tx and Rx electrodes.

difference exists at lower frequencies. However the difference value is proportional to the applied signal frequency as shown in figure 3.13. A gain difference of ≈3dB at 49 MHz is shown as D_s increased from 10cm to 13cm, yet as the transmission distance is increasing at the same frequency, the same gain value difference is obtained.

Inter-electrode Spacing Effect

This separating distance is essential to produce a potential difference at transmitting electrodes side and to detect the potential difference at receiving side. Figure 3.12 shows the

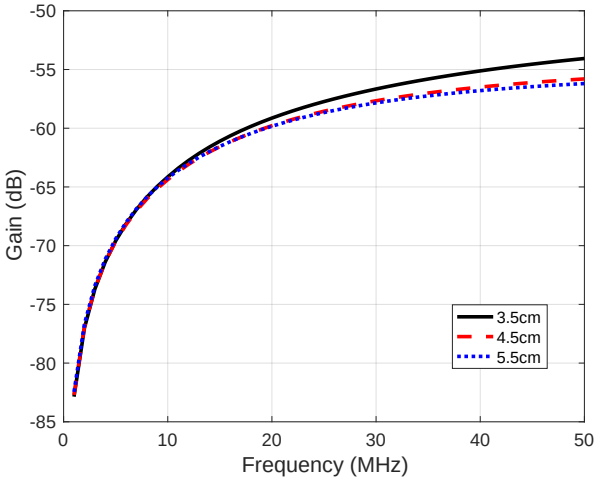

Figure 3.14: The influence of inter-electrode spacing is shown in terms of gain values by varying the separation distance between transmitting electrodes terminals and receiving electrodes terminals.

breaking distance within the transmitting and receiving terminals which is denoted as L_T and L_R, respectively.

By increasing the inter-electrode distance from 3.5cm up to 5.5 cm with a step difference of 1 cm, transmission gain values change is clear as shown in figure 3.14. The maximum inter-electrode distance of 5.5cm showed the highest gain at frequency range between 1MHz-10MHz. However, all higher frequencies demonstrate that inter-electrode spacing of 3.5cm has the highest gain values over 10MHz.

Mono Inter-electrode Spacing Effect

After investigating the effect of inter-electrode spacing variation in both the transmitting and receiving terminals, it becomes intriguing to study the effect of manipulating the inter-electrode separation of one side of the IBC communication system. This can be achieved by only changing the spacing of Tx, which is denoted as L_T as shown in figure 3.12, wherein L_R of Rx remains fixed, e.g. L_R= 3.5cm, and vice versa.

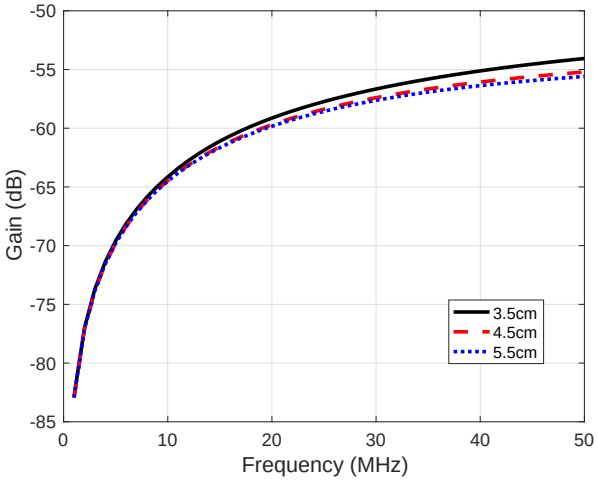

Figure 3.15: The influence of Tx inter-electrode spacing is shown in terms of gain values by varying the separation distance between terminals of transmitting electrodes .

By increasing only the separation distance of Tx terminals, higher performance degradation occurs as the injected alternating current suffers greater inter-electrode impedance value which lead to an attenuation to the body confined electromagnetic propagation with respect to all chosen frequencies of operation as shown in figure 3.15. However, augmenting exclusively the spacing of Rx mitigates the detection of traveling signal at lower frequencies since longer wavelength of propagated signal is evident as shown in figure 3.16.

Impact of Electrodes Dimensions

One of the factors to optimize the IBC system is by selecting the proper dimensions of coupling and detecting electrodes. The transmission distance and inter-electrodes separation are fixed to the values in the previous setup section wherein the geometry of electrodes are determined to be square shaped. The height of the electrodes is irrelevant to system performance yet a height of 5mm is determined for simpler FEM design.

The variation of electrodes' dimensions has been investigated between 13-19mm as shown in figure 3.17. Clearly the electrodes with sides of 15mm prove to have the highest transmission

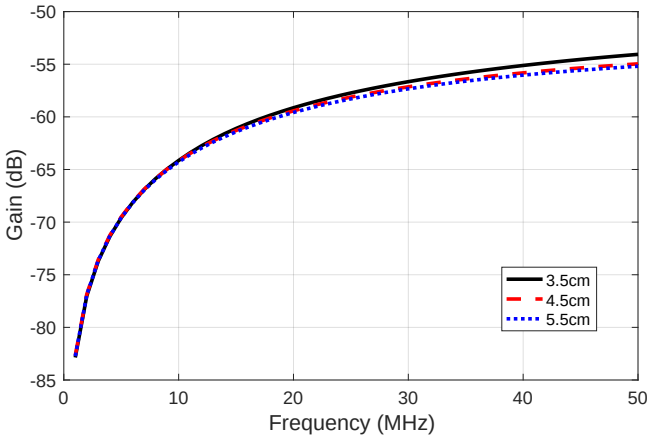

Figure 3.16: The influence of Rx inter-electrode spacing is shown in terms of gain values by varying the separation distance between terminals of receiving electrodes.

gain with respect to all determined signal frequencies. These results are explained in terms of capacitive and current terms. As the sides of electrodes decreases below 15mm, a decrease in the coupling area of electrodes arises. On the other hand, the dimensions of the electrodes is inversely proportional to the transmission gain above the 15mm sides of electrodes duo to an increase in parasitic capacitance between Tx and Rx terminals. Also current leakage between electrodes may occurs as the sides of the electrode are increasing.

Although the dimension of electrodes are preferred to be smaller to ensure user comfort, a trade-off to system performance has to be considered. Still, the shown optimum dimensions are very suitable for IBC applications.

Conductivity Effect on Transmission Gain

The importance of tissues' dielectric properties lays on its influence on the performance of IBC system. As seen in figure 3.4, the muscle tissue has the highest values of conductivity σ_m wherein the skin tissue shows lower conductivity σ_s readings in both conditions of wet and skin status. Due to high conductivity, muscle layer has a crucial rule on transmitting the

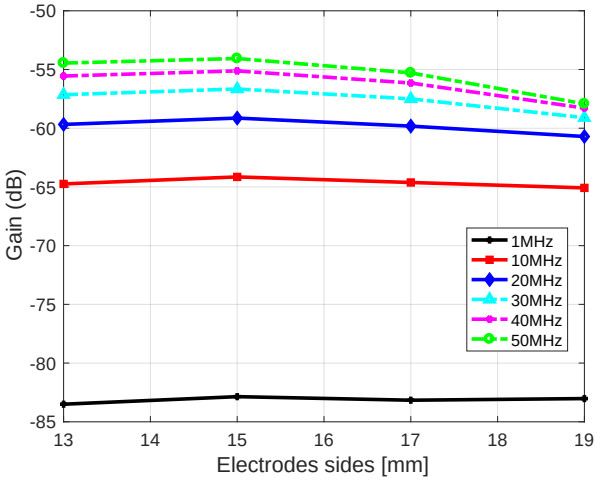

Figure 3.17: Varying the sides of the squared coupling and detecting electrodes results in gain values variation where the gain of 15mm electrodes' sides is the highest.

inject current. Nonetheless, skin tissue is on direct contact with the coupling and detecting electrodes. In addition, skin layer has good conducting characteristics. Other tissues such as fat and cortical bone prove to have much lower conductive property hence investigating its effect on system performance is discarded.

By altering the values of imported conductivity values of skin and muscle tissues by an order of 10, the influence is apparent as shown in figure 3.18. When changing the magnitude of conductivities, the skin tissue proves to have a significant impact on transmission gain values, e.g. increasing by an order of 10 improved the gain values by $\approx$ 5dB at 40MHz. In contrast, modifying the conductivity of muscle tissue to investigate its influence can be neglected since gain values difference is not evident as shown in figure 3.18.

The impact of tissues' conductivity property manifests on ions flow in order to transmit the coupled signal between Tx and Rx. This property is inversely proportional to the transversal impedance, which is described at 3.9, that impedes injected current flow to be transmitted. By increasing σ_s, skin tissue's path becomes dominant in conducting the coupled signal which saves the injected current from flowing throw the less conductive fat tissue. In contrast, when decreasing σ_s, the skin which is directly adhered to electrodes act as a barrier that prevents

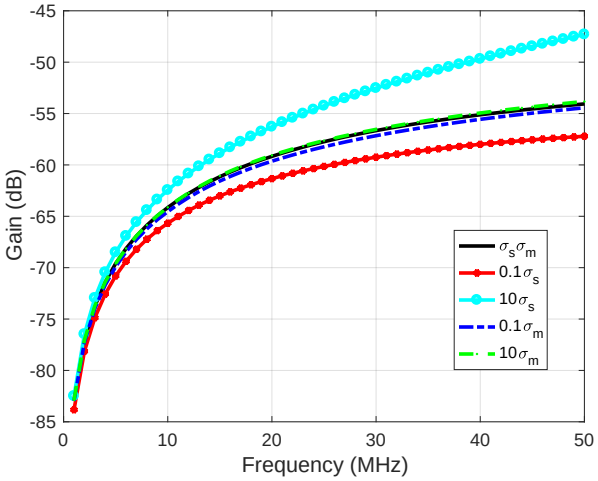

Figure 3.18: Reducing and incrementing the conductivity of skin and muscle tissues by an order of 10 influences the performance of IBC system.

the signal from flowing though the body. Although muscle's higher conductivity compared to skin layer has an important rule on current flow through human channel, increasing shows minor enhancement on gain values due to the tendency of current to flow within lower layers of human channel in this case. Moreover, decreasing σ_m proves to have typical influence as in the prior case but with negative impact on gain values.

3.4.3 Model Validation

To verify the simulation results of simplified cylindrical arm model and full human arm model simulated on ANSYS, path loss readings of analytical model are included as shown in figure 3.19. The detailed geometry of human arm model which includes veins, uneven thicknesses of muscle and bone layers, the nonuniform surface of skin that affects the positioning of all electrodes structure play a main role in the observed difference of gain values between human and cylindrical model. However, results show that using cylindrical model can be an alternative to using a model with detailed human geometry when targeting less accurate yet fast results of path loss profile as the difference of gain is at its maximum at 9.5MHz with transmission gain variation of 4dB which is decreasing at lower and higher frequencies.

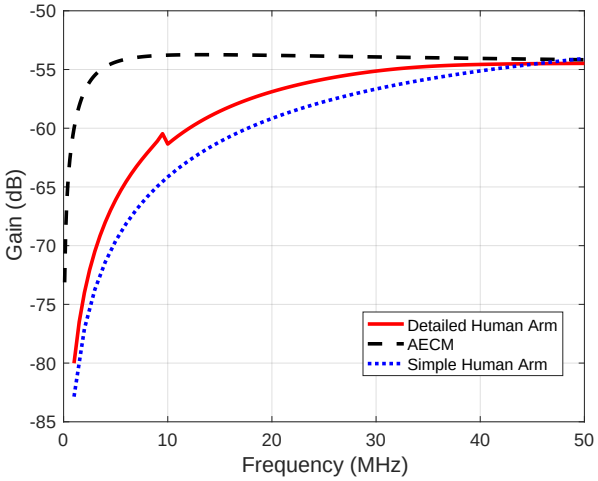

Figure 3.19: Transmission gain in (dB) of the analytical equivalent circuit model of the arm, ANSYS detailed arm and ANSYS simplified arm.

Full arm model and simplified arm model compared to analytical model show a high gain difference at lower frequencies. However, at higher frequencies between 40-50MHz, analytical, detailed and simplified arm human models exhibit an agreement in pass loss. Factors that contribute to the difference between AECM and ANSYS models include neglecting the coupling impedance of transmitting and receiving electrodes in AECM derivation in order to simplify calculations which is observed at lower frequencies. In addition, the derived electrodes' model of AECM, the meshing convergence procedure of FEM simulation and electrode internal impedance are factors in data variations.

The coupled EM signal creates two current components described as conduction and displacement current [40] [32]. The conduction current at lower frequency which results from flow of charges is high. Consequently, coupled signal is confined within the human tissues and therefor leads to higher detected signal at Rx electrodes. The conduction current can be described in the following

$$I_c = GV \tag{3.11}$$

where G is the conductance and V is the initiated voltage in a unit volume of human tissues.

Table 3.1: CPU time of AECM, simplified and detailed arm simulations.

Model	**CPU time (hh:mm:ss)**
ECA	(00:00:1.62)
FEM of cylindrical arm	(00:02:56)
FEM of human arm	(01:37:29)

However, at higher frequencies, conduction current remains constant and the capacitive effect becomes dominant which results in a continuous increase in displacement current. This phenomenon leads to signal dissipation into the surrounding environment which eventually decreases the intensity of the received signal. The displacement current can be characterized in the following

$$I_D = -\omega C V_o sin(\omega t) \tag{3.12}$$

where ω is the angular frequency of the applied current, C is the capacitance and V_o is the initiated voltage corresponding to a unit of the human tissues. From figure 3.19, we observe the effect of displacement current at 49 MHz of detailed human arm readings.

3.4.4 FEM and ECA simulation time

The required simulations have been completed on a common computing setup. Simulations were performed using a quad core processor running at 2.3 GHz with 8 GB of RAM.

Simulation time is calculated in terms of CPU time to determine the required time for the central processing unit to complete each simulation. Table 3.1 summarizes the estimated CPU time for each model simulation Clearly, the total CPU time of the detailed human arm FEM simulation is $\approx$ 48 times the estimated time in case of simplified cylindrical arm. As expected, ECA model shows the fastest simulation time.

3.4.5 Current Density Distribution

In the galvanic coupling approach, the coupled electromagnetic signal exhibit dipole type field behavior [41]. This field can be represented in terms of current density vectors to show current paths along multiple tissues. Current paths are mainly composed of primary path that flows between the transmitting electrodes and secondary path the results in potential difference between the receiving electrodes as shown in figure 3.20. The source electrode current exciting the primary and secondary flows is as follows

$$I = \iint_s J.ds = \iint_s \sigma.E.ds \tag{3.13}$$

where J ($\frac{A}{m^2}$) is the current density and s is the surface area of Tx electrode and E is the normal electric field intensity component between the contact area of Tx and skin tissue [32].

The value of current density distribution within the five main human layers is affected by the relative permittivity and conductivity of these tissues. These parameters' contribution on current density has been investigated by simulating a 1mA coupled current at 49MHz. The skin layer has higher σ than fat tissue. Due to this fact, current density distribution values in skin is higher than observed values in fat, which can be observed in figure 3.21 and figure 3.22. Moreover, we can notice that the values of J along the muscle tissue are higher than fat layer. The conductivity of muscle tissue, which is the highest compared to the other layers, is the reason behind this observation as the primary current of coupled signal penetrates through the fat tissue located under Tx electrodes and easily transmitted along the muscle tissue. Finally, the current distribution has been plotted along bone marrow tissue to verify the impact of its low conductivity property as shown in figure 3.24.

In addition, the amount of movable charges between Tx and Rx electrodes are impacted by the described impedances in the previous sections. For instance, in case of longitudinal transmission for wearable sensors, transverse impedance Z_t is affected by the value of corre-

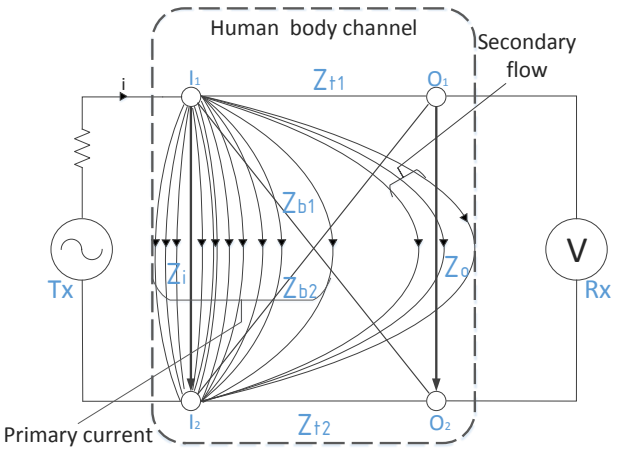

Figure 3.20: Current flow paths of galvanic coupling.

sponding tissue's conductivity. As σ_n increases, Z_t decreases which leads to higher values of detected potential difference.

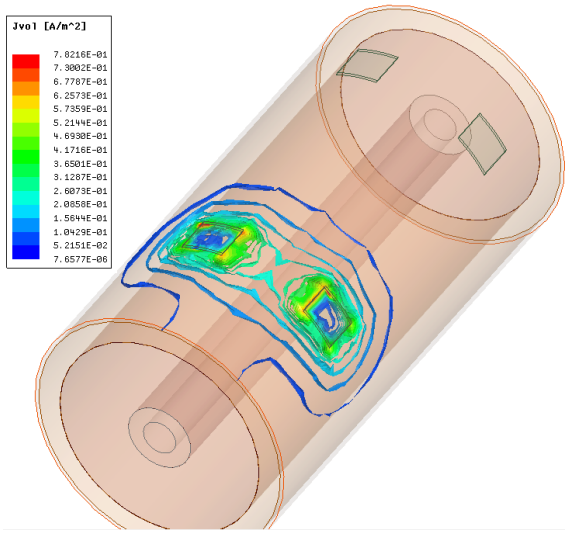

(a) Primary current distribution

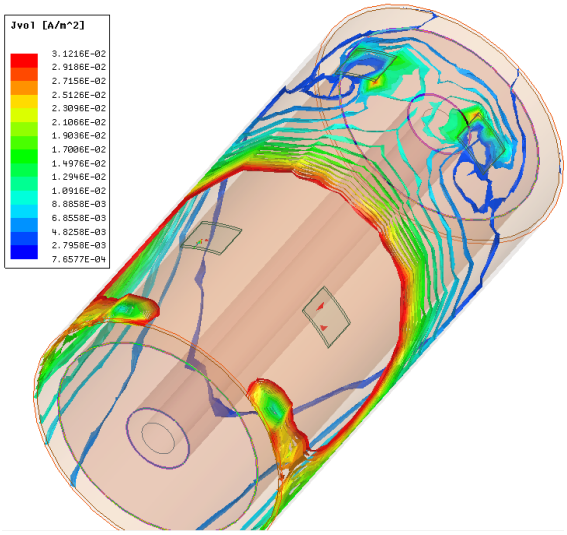

(b) Secondary current distribution

Figure 3.21: Skin tissue's current density distribution.

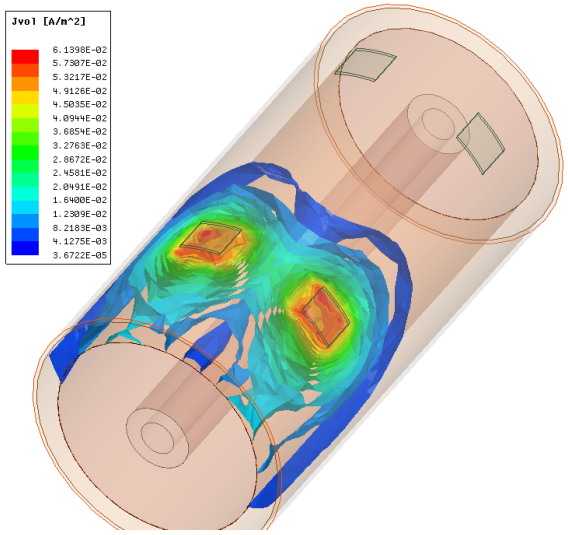

(a) Primary current distribution

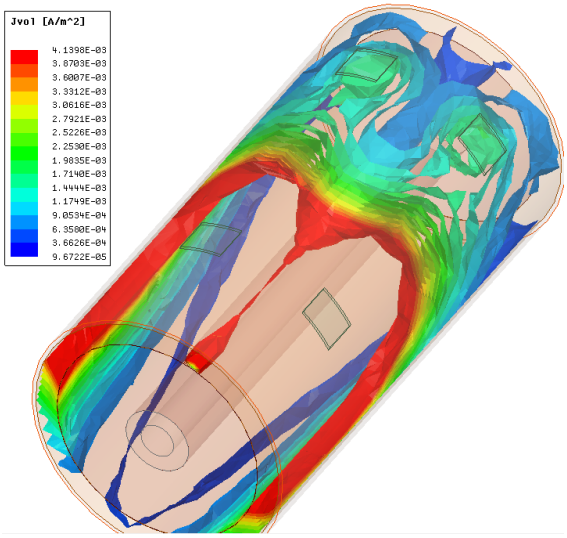

(b) Secondary current distribution

Figure 3.22: Fat tissue's current density distribution.

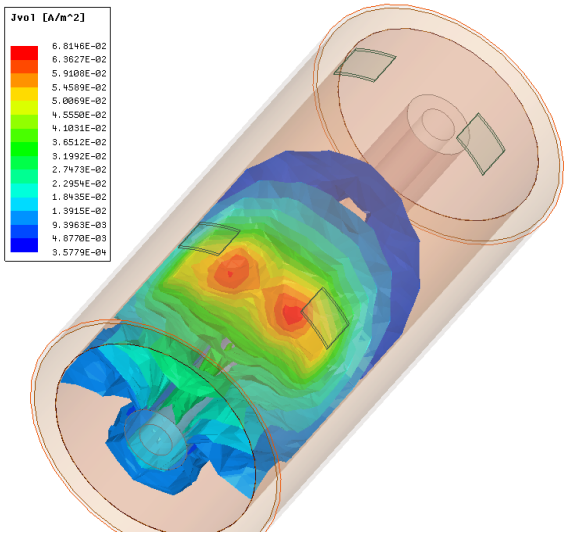

(a) Primary current distribution

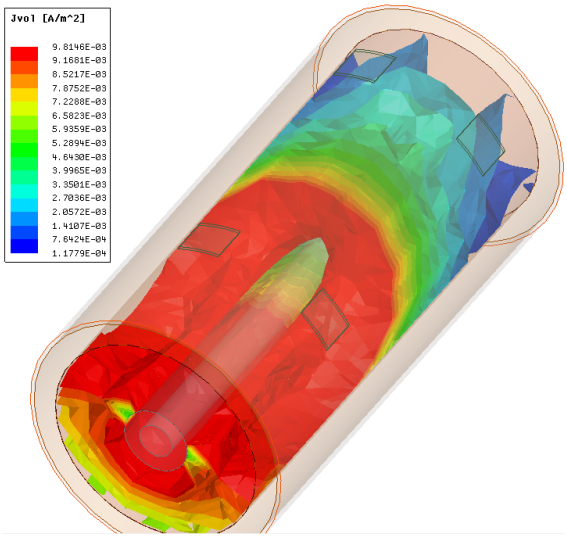

(b) Secondary current distribution

Figure 3.23: Muscle tissue's current density distribution.

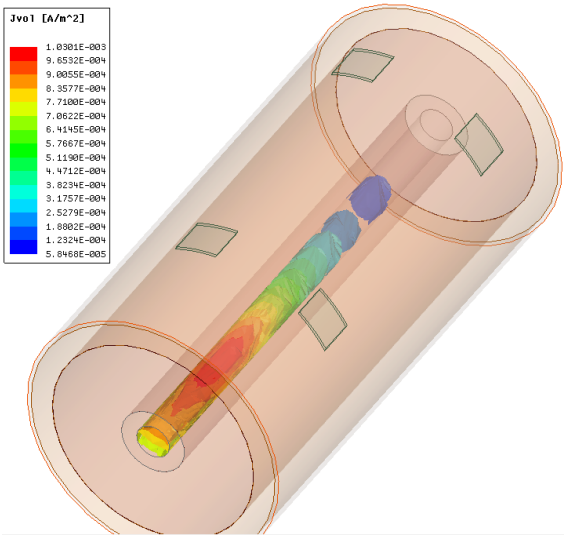

(a) Primary current distribution

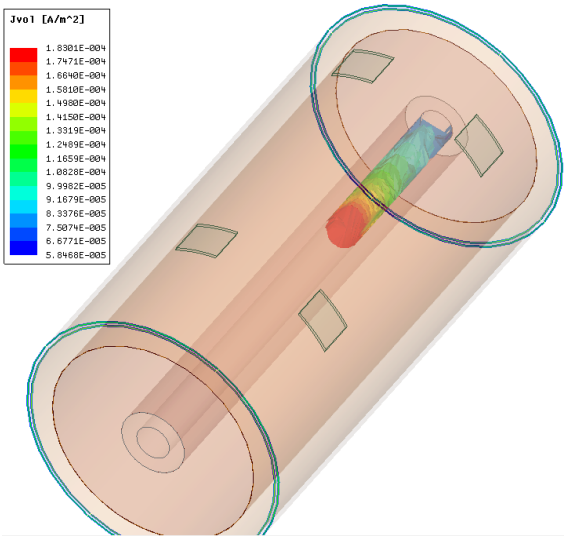

(b) Secondary current distribution

Figure 3.24: Bone marrow tissue's current density distribution.

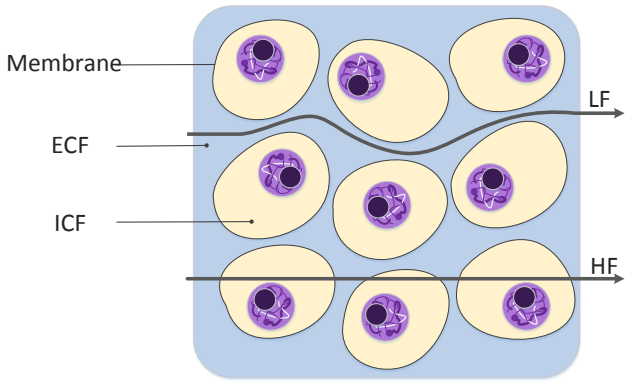

Figure 3.25: Alternating current behavior with respect to frequency value alongside tissue content.

Cell Content Affect on Current Flow

The main component of human body organs and tissues are cells that sustain biological processes. Each cell is confined internally by a surrounding fluid called intracellular fluid (ICF) where this fluid is enclosed by a membrane. These cells are also surrounded by another fluid called extracellular fluid (ECF) [42]. By exciting the biological tissue with an alternating current, two current trends are observed as shown in figure 3.25.

In case of low frequency current such as 1KHz, the high impedance of the cell membrane forces ions flow to be limited only to the extracellular fluid areas. The isolating nature of the cell membrane between two conducting mediums, manifest in ICF and ECF, exhibit a capacitor behavior within the biological tissue. As a result, coupling a high frequency signal, such as 49 MHz, facilitates current flow within both surrounding fluids as the reactance of the membrane is at minimum [43]. However, increasing the frequency of the injected current is bounded to a frequency limit where surpassing it may result in other factors that contribute to signal scattering outside of the human body such as the previously discussed case of displacement current.

Figure 3.26 shows the effect of decreasing the frequency of injected current from 49MHz, as shown in figure 3.21, to 1MHz along skin tissue. At later frequency, it is clear to observe

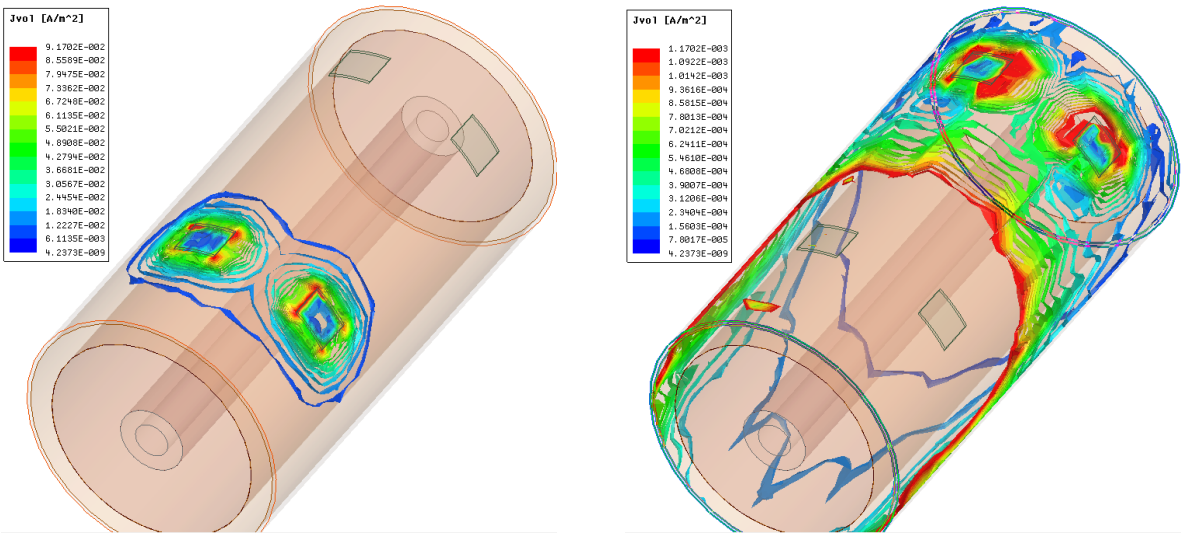

(a) Primary current distribution (b) Secondary current distribution

Figure 3.26: Skin tissue's current density distribution at injected current frequency of 1MHz.

Table 3.2: Properties of DCP.

Plate Material	**Length**	**Width**	**Hole Spacing**
Stainless steel Titanium	25mm to 145mm	10mm	12 and 16mm

the reduction in current density readings since higher tissue impedance obstruct ions flow at lower frequencies.

3.5 Internal Fixation Implant Effect

Bone fractures are one of the most common injuries that requires immediate care. The typical procedure for dealing with these fractures is by using an implant that can attach both broken parts of the bone for a long time that can take up to several weeks until both separated parts of the bone are healed and attached together. In this section, we investigate the effect of this implant by using the modified concentric cylinders as shown in figure 3.27. Dynamic compression plate (DCP) is a conventional choice by orthopedic surgeons to compress and stabilize bone fractures [44]. The plate has a spherical gliding

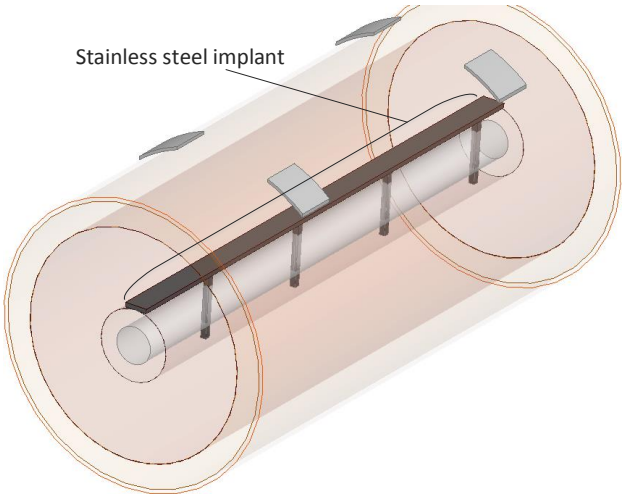

Figure 3.27: The simplified human arm model including an internal fixation implant.

holes which allows the spherical headed screws to have a self compression effect. Table.2 describes the characteristics of (DCP) [45].

By exciting the electrodes of the arm model which includes the implant, it has been noted that path loss increased by about 0.5 dB, which can be seen in figure 3.28. Since DCP is adjacent to cortical bone and all electrodes are on skin layer, the plat can have an effect of a sink point that reduces the detected potential difference by Rx electrodes, hence transmission gain.

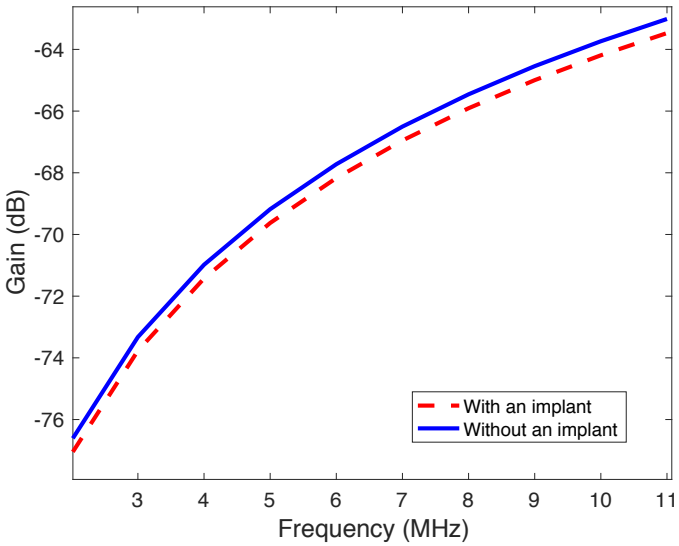

Figure 3.28: The simulation results of the cylindrical arm model with and without DCP.

Chapter 4

Human Phantom[1]

4.1 Introduction

The most accurate and reliable approach to validate the outcome of human channel estimation simulations is by conducting the same transmission setup on the human body. However, the deficiency of participants' number forms an obstacle in evaluating the effect of geometrical and biological variance between each individual. In addition, performing repeated measurements on the same participants for a wide spectrum of volunteers is not easily obtainable. Also, conducting experimental measurements on human subjects is susceptible to any setup error which may result in catastrophic accidents. Therefore, to overcome these issues, developing a human phantom that mimics the dielectric properties of the human body is preferred to replace the human body.

The main advantages of the human phantom are relative to the application. For IBC, the flexibility of the phantom facilitates fabricating arm phantoms with different diameters and dimensions in order to investigate the influence of varying arm's dimensions on the transmis-

[1]This chapter's experiments are cooperative work with Ahmed E Khorshid.

sion of coupled signal. Moreover, since the arm phantom preserves its dielectric properties for long-term, it enables applying many repeated experiments on the same phantom without the need to fabricate a new one which benefits in saving time and minimizing experimental fabrication error.

When choosing the phantom that is suitable for the IBC application, three parameters have to be considered:

- Dielectric properties
- Stiffness
- Longevity

As mentioned before, the main advantage of the phantom is its ability to mimic the dielectric and electrical properties of the human body. Therefore, the closer the values of permittivity and conductivity of the phantom to the human body, the more accurate the phantom is. In addition, in order to build an arm phantom with five layered tissues, the structure of the phantom has to be rigid enough so that none of the phantom tissues will mix which certainly will happen when using a liquid phantom such as the case in [25][46]. Finally, the longevity of the phantom has to be long enough to conduct repeated experiments without the need to rebuild another phantom within a short period of time, e.g. it has to last for at least a month before losing its dielectric properties values.

4.2 Preparation

In order to satisfy the previous requirements of the phantom, two methods of fabrication are conducted. The following subsections include details of the materials and preparation steps of each fabricating method.

Table 4.1: Detailed quantities of required materials for fabricating oil samples.

Material	**10%**	**20%**	**30%**	**40%**	**50%**	**60%**	**70%**	**80%**	**90%**
Safflower oil (ml)	19.4	43.75	75	116.7	175	262.5	408.3	700	1575
Surfactant (ml)	0.2314	0.48125	0.825	1.2837	1.925	2.8875	4.4913	7.7	17.325
Bloom gelatin (g)	26.95								
Propylene Glycol (g)	10.5								
Deionized water (ml)	169								
Formaldehyde (g)	1.323								

4.2.1 Oil

The main preparation steps of the first fabricating method are adopted to construct the human arm phantom [47]. Table 4.1 describes the weights and volumes of each required material for the phantom samples where oil is the main component of fabrication. The main changes of materials quantities are concluded by fixing the amount of materials other than oil and surfactant. The reason behind that is oil plays a main rule in altering the phantom dielectric properties, hence oil quantity change is described in terms of different concentrations as shown in table 4.1. In addition, volume of surfactant or "ultra ivory" has to be enough to ensure oil dissipation and blending within the remaining mixture. The bloom gelatin plays a main role in making the structure of the phantom rigid.

After collecting all required materials and preparing an appropriate experimental setup, the preparation steps are performed as shown in figure 4.1. The most crucial part of the experiment is cooling down and keeping the heat of the mixture constant to 50^{o}C while heating up the required oil to be added to the mixture. If this step is not successful, the oil will not dissolve within the mixture which calls for repeating the experiment. Finally, the complete mixture is poured into a mold and preserved for at least 8 hours before further experimental applications.

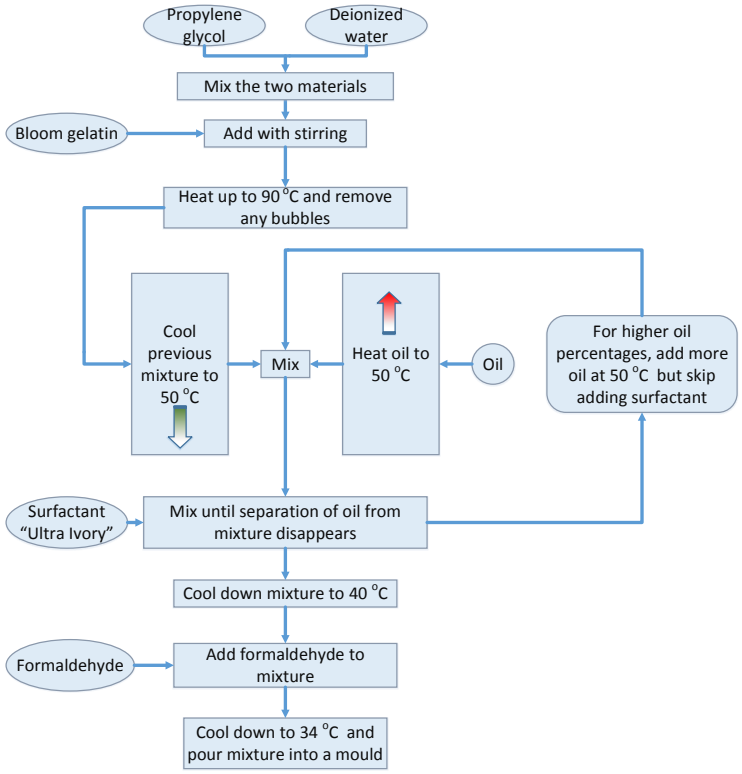

Figure 4.1: An outline of the preparation steps for the oil only samples.

4.2.2 Oil and Kerosene

Another fabrication method of the arm phantom is adopted in this thesis with an alternative method of calculations by mainly including kerosene into the oil mixture [48]. Although only the oil, including kerosene, and the surfactant are changing in weights for all required concentrations along all materials, few changes in phantom materials are observed, e.g. n-propanol. In addition, since this experiment requires the use of kerosene which is highly flammable, more precaution steps are necessary to ensure the safety of the experiment setup.

Each oil concentration includes variation of oil mixture which contains 50% of safflower and 50% of kerosene. Table 4.2 includes detailed description of the essential materials' weights and volumes. Oil concentration of 90% is not included in calculations since the total volume in this case is above the capacity of our lab tools. The flow of preparation steps is shown in figure 4.2.

Table 4.2: Detailed quantities of required materials for fabricating oil and kerosene samples.

Material	10%	20%	30%	40%	50%	60%	70%	80%
Oil and kerosene (ml)	22.2	50	85	133.3	200	300	466	800
Surfactant (ml)	1.26	2.8	4.76	7.46	11.2	11.2	11.2	11.2
Bloom gelatin (g)	34							
N-propanol (ml)	10							
Deionized water (ml)	190							
Formaldehyde (g)	2.16							
P-toluic acid (g)	0.2							

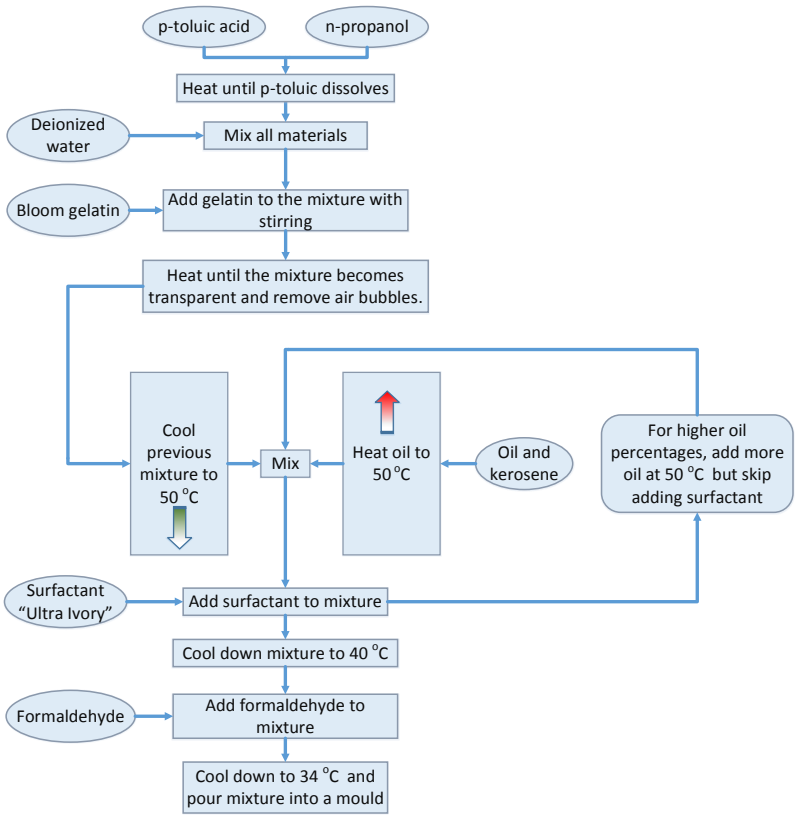

Figure 4.2: An outline of the preparation steps for the oil and kerosene samples.

4.3 Results

After the molds are ready for measurements, small samples are cut and placed in the impedance analyzer in order to collect the dielectric properties of each sample. The final values are averaged and plotted along the human arm values for the purpose of matching the correct oil concentration with the body tissue. The electrical properties of oil only samples are shown in figure 4.3 and figure 4.4.

Clearly, the values of the oil only permittivity has the same exponential behavior as in the case of the arm tissues which are shown in figure 4.3a. For better view, all oil only concentrations' permittivities are plotted as shown in figure 4.3b. The same matching procedure is applied for the conductivities values as shown in figure 4.4. However, we can observe that all conductivity values of oil concentrations have the tendency to a linear behavior along all frequencies which is not the case of the high pass filter behavior in the human tissues. Yet, at higher frequencies, all conductivity values can be matched to the oil phantom.

The combination of oil and kerosene along with the remaining materials altered the values of permittivity and conductivity compared to the case of oil only phantom, e.g. at 10% oil and kerosene concentration the highest value of permittivity is 350 which was over 500 in case of oil only phantom. The dielectric properties of oil and kerosene phantom are shown in figure 4.5.

It is crucial to find an easy and reliable technique that facilitates the matching process between all oil concentrations and human arm tissues' electrical properties. In this thesis, the experimental measurements error formula is utilized to achieve this process. The measurements error defines the difference in values of electrical properties between each oil concentration and every arm tissue. Figure 4.6 shows an example of measurement error in case of cortical bone conductivity matched to 60% oil. Finally, after obtaining the matched oil concentrations, a full arm phantom can be fabricated for further IBC's measurements.

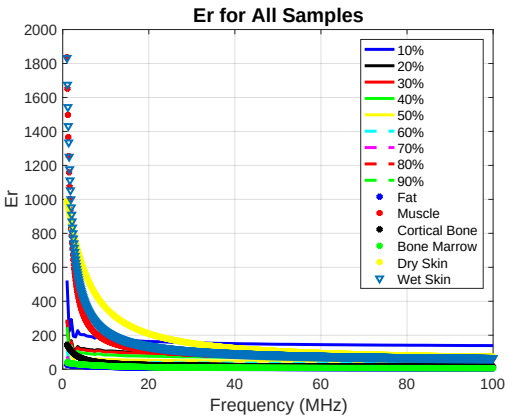

(a) Readings compared to human measurements

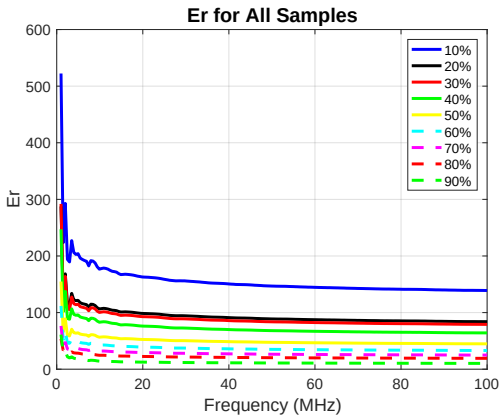

(b) Permittivity readings

Figure 4.3: The measurements of permittivity values for all oil only concentrations

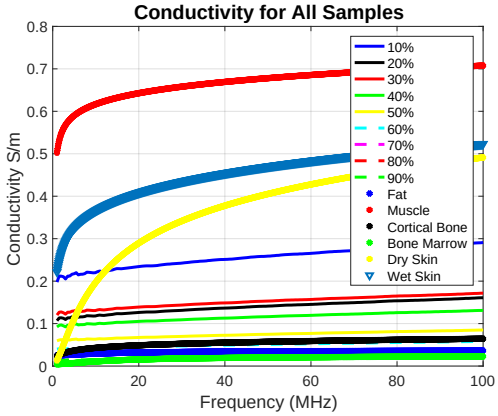

(a) Readings compared to human measurements

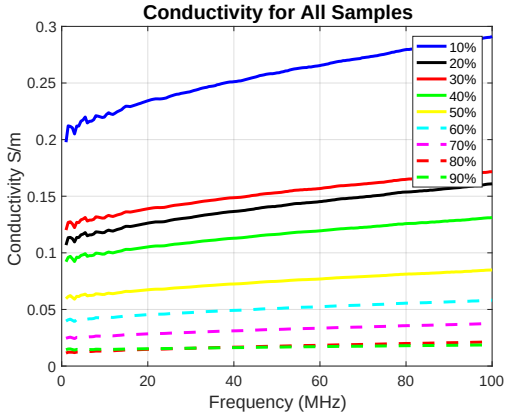

(b) Conductivity readings

Figure 4.4: The measurements of conductivity values for all oil only concentrations

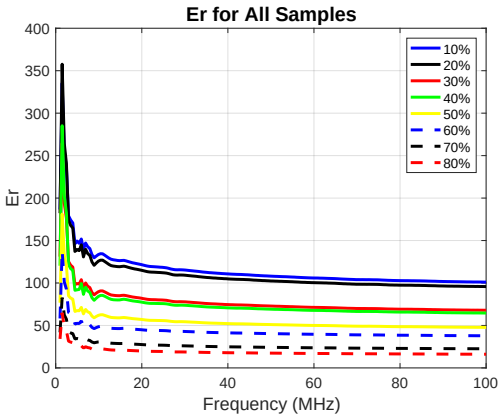

(a) Permittivity readings

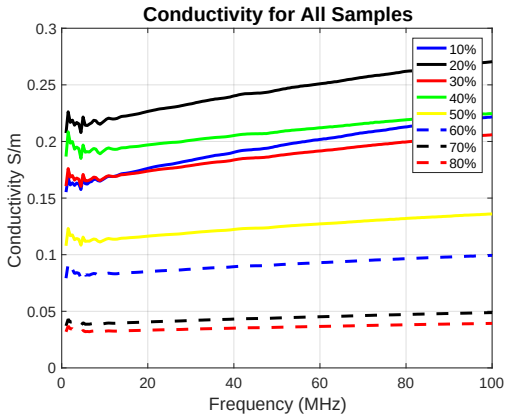

(b) Conductivity readings

Figure 4.5: Dielectric properties of oil and kerosene samples.

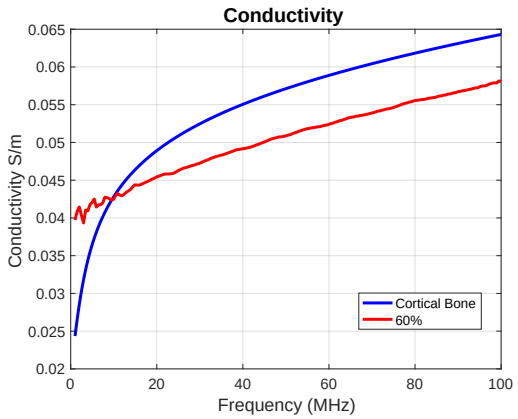

(a) Conductivity comparison

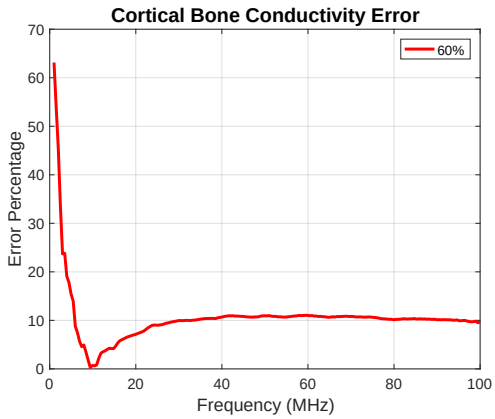

(b) Error calculation plot

Figure 4.6: The matching between conductivity values of cortical bone and oil only concentration of 60% is based on the minimum measurement error acquired along all oil concentrations.

4.3.1 Dual Integrated Molds

Before moving into the full arm phantom fabrication, it is required to investigate if there is any dielectric properties influence of composing a phantom with random oil concentration to be adjacent to another phantom with different oil content. This approach enables us to predict the effect, if there is any, of oil phantoms on each other in order to solve any resulting obstacles before building a complete arm phantom.

For this subsection, 60% of high oil and kerosene content has been chosen to surround a centric oil and kerosene mold with low 20% concentration as shown in figure 4.7a. The 60% concentration can only be poured next to 20% after five days to ensure all materials interactions.

The most important mold samples are the ones co-located between the 20% and 60% phantoms which are denoted as "separated samples" in figure 4.7b. The influence in dielectric properties is minor as shown figure 4.8 where "separated samples" are compared against an "only 20%" samples and lastly against a different mold of 20% that was prepared a week before labeled as "12,12".

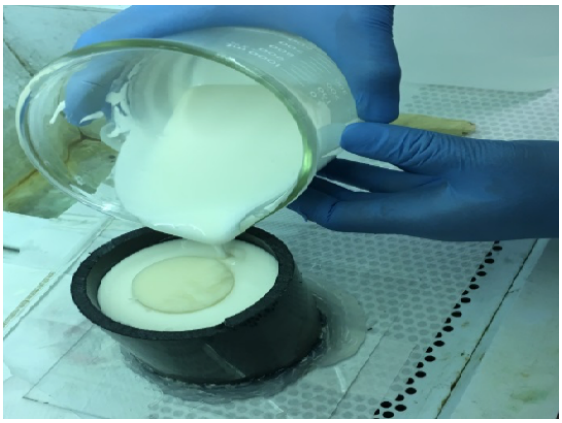

(a) Mold fabrication

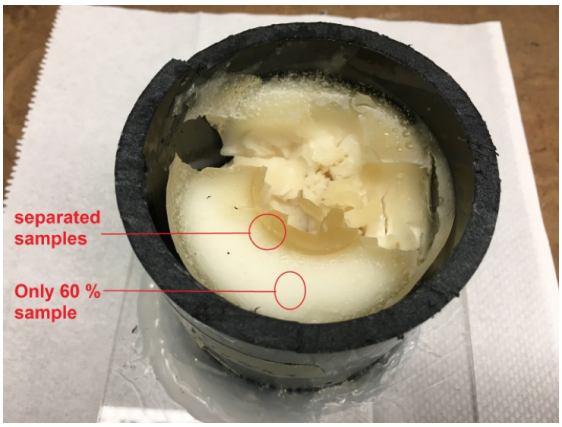

(b) Labeled samples for clarification

Figure 4.7: The shape of the integrated mold before and after collecting samples for dielectric properties measurements wherein the center cylinder is for the 20% oil and kerosene concentration and the surrounding cylinder is for the 60% oil and kerosene concentration.

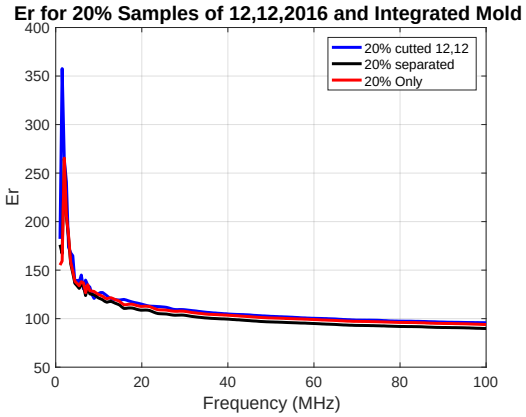

(a) Permittivity readings

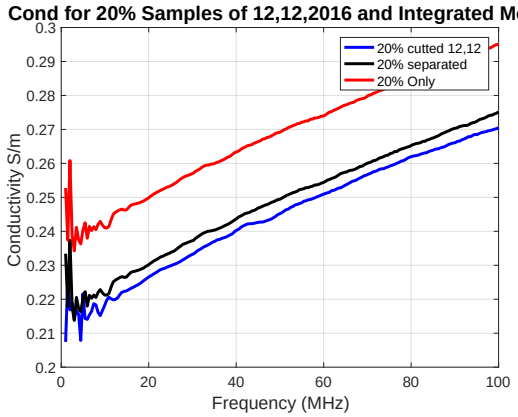

(b) Conductivity readings

Figure 4.8: Comparison of dielectric properties values between dedicated oil and kerosene samples and integrated oil and kerosene samples wherein the concentration of oil in both cases is 20%.

Table 4.3: The detailed quantities of materials needed for muscle and skin phantom fabrication.

TX-150 (g)	Aluminum (g)	Water (ml)	NaCl (g)
33.92	25	283.08	0.98
	10		
	5		

4.4 Phantom of Muscle and Skin Tissues

Unfortunately, the electrical properties of both oil phantoms can not be matched with the muscle and skin tissues due to the large difference in measurements. The skin and muscle tissues play a main rule in transmitting the coupled galvanic signal of IBC. Therefore, it is necessary to find other phantom materials that are able to mimic the properties of both crucial arm tissues. This section introduce a replacement to overcome this issue by mainly using aluminum powder [49].

4.4.1 Preparation

In addition to the dielectric values of this phantom, the small number of the required materials, as shown in table 4.3, and the short preparation steps facilitate the whole experiment to be faster and easier to conduct. However, important precaution standards have to be followed when depositing the aluminum powder into the prepared mixture. The particles of the aluminum powder, which are smaller than sand particles, can easily spread and scatter into the air without careful movement when taking a scoop of aluminum out of its container.

After weighting and preparing all needed materials, the first step comes by mixing the aluminum with a gelling agent indicated as TX-150 as shown in figure 4.9. The shear stirrer is essential to ensure interaction of aluminum particles with the remaining materials. After the final step, the phantom can be used for further applications after few hours of reservation.

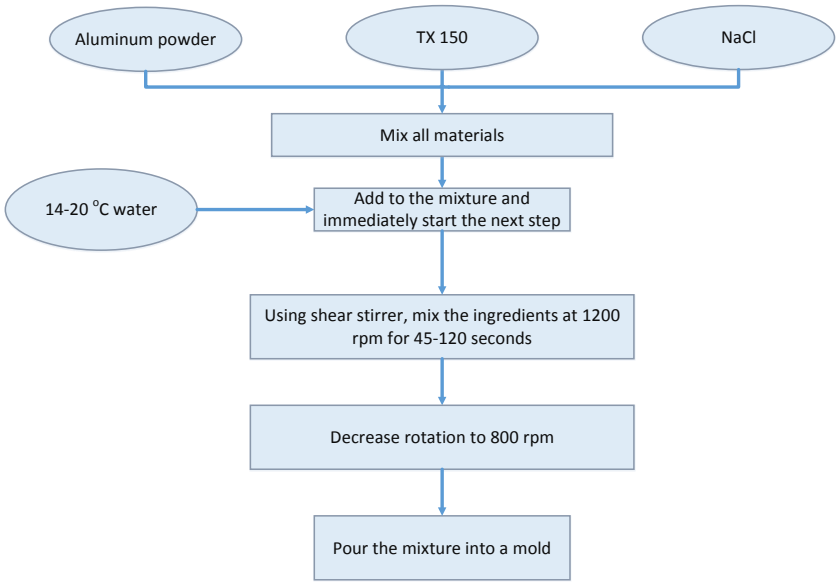

Figure 4.9: An outline of the fabrication steps for Tx-150/aluminum phantom that mimics properties of muscle and skin tissues.

4.4.2 Results

The variations of aluminum weights exclusively incorporated in dielectric properties' values changes. These weights alterations resulted in great muscle permittivity matching when selecting aluminum weight of 10g as shown in figure 4.10a. Moreover, the conductivity readings difference has decreased significantly when using the same previous weight of aluminum as shown figure 4.10b.

In addition to the muscle tissue, the dielectric properties of the skin tissue, in wet condition, are matched to the aluminum phantom. The values of the wet skin permittivity are approximately equal to the permittivity of the 10g aluminum. Also, the conductivity values of wet skin is nearly between the conductivity values of both 5g and 10g of aluminum. These results suggest selecting an aluminum weight of 8g which can decreases the difference to the minimum.

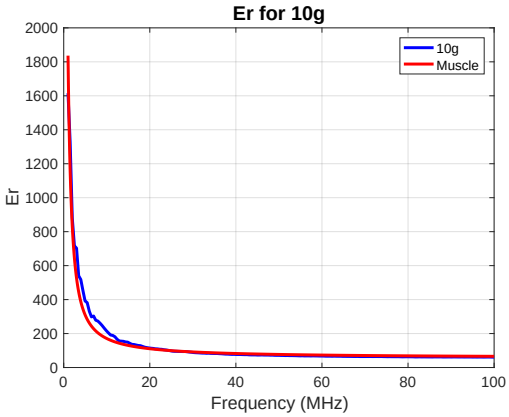

(a) Permittivity readings

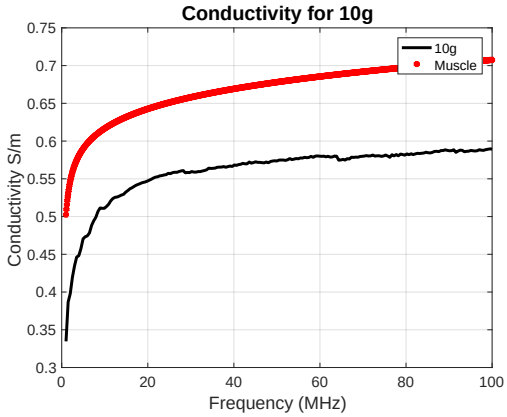

(b) Conductivity readings

Figure 4.10: It is clear that the accuracy of the muscle tissue dielectric properties matching has improved significantly when using TX-150/aluminum phantom.

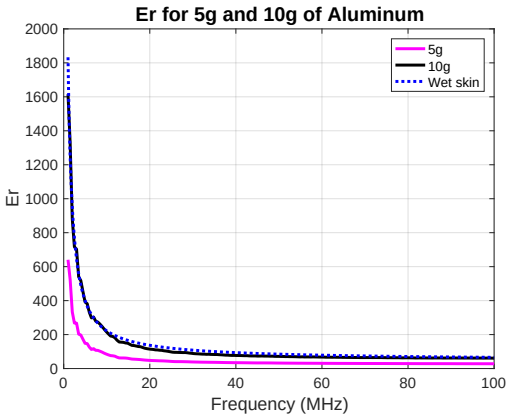

(a) Permittivity readings

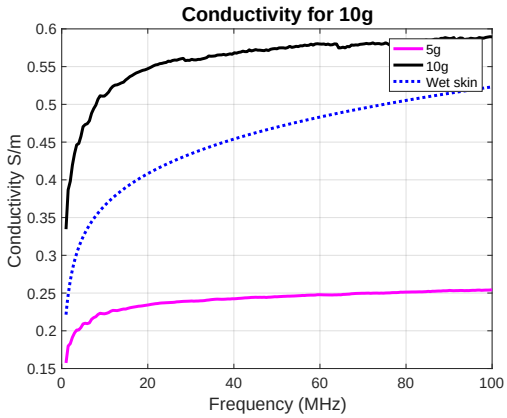

(b) Conductivity readings

Figure 4.11: The conductivity readings of both aluminum weights are not matched with the wet skin readings, yet the measurement has improved significantly when using TX-150/aluminum phantom instead of oil phantom.

Table 4.4: Final required phantoms for each tissue of the complete human arm.

Tissue	**Type of phantom**	**Concentration or weight**
Bone marrow	Oil only	80%
Cortica bone	Oil only	60%
Fat	Oil and Kerosene	80%
Muscle	Aluminum	10g
Skin	Aluminum	8g

4.5 Conclusion

This chapter discussed several phantom preparation methods in order to fabricate a full human arm phantom. Despite the differences in making all presented phantoms, every technique participates in dielectric properties matching to a human tissue. Table 4.4 summarizes the matched phantoms to each human arm layer for the targeted purpose of eventually fabricating a full human arm and conducting galvanic IBC applications.

It has to be mentioned that final decision of choosing the appropriate phantom was more focused on conductivity values matching more than permittivity values for each tissue. Our theoretical calculations of derived transfer function showed higher sensitivity to conductivity values rather than permittivity. Moreover, since the highest gain in the presented simulations of this thesis is located at transmission frequency of 49MHz, the error has to be at minimum for all tissues' phantoms along the same frequency.

As the arm phantom contains five different layers, fabrication process has to be planned in advance by calculating the total required weights of materials to avoid exposing some of the layers to air for long time. The total required time to complete the full arm is averaged to a week of phantoms making.

Bibliography

[1] Yong Song, Qun Hao, Kai Zhang, Ming Wang, Yifang Chu, and Bangzhi Kang. The simulation method of the galvanic coupling intrabody communication with different signal transmission paths. *IEEE Transactions on Instrumentation and Measurement*, 60(4):1257–1266, 2011.

[2] How to read brain activity?, author = Tbingen, Max Planck Campus, year = "2016 (accessed: 2017- 09- 07)", howpublished = `https://tuebingen.mpg.de/en/detail/how-to-read-brain-activity/`.

[3] PS4 VR headset price REVEALED on Amazon - and it's NOT good news, author = Express.co.uk, year = "2016 (accessed: 2017- 09- 07)", howpublished = `http://www.express.co.uk/life-style/science-technology/632733/sony-ps4-playstation-vr-headset-uk-price-release-date`.

[4] ECG Electrode, author = , year = "2008 (accessed: 2017- 09- 07)", howpublished = `https://dir.indiamart.com/impcat/ecg-electrode.html`.

[5] sugarBEAT Continous Glucometer Cleared in Europe —. `https://www.medgadget.com/2016/03/sugarbeat-continous-glucometer-cleared-in-europe.html`, 2016 (Accessed: 2017- 09- 07).

[6] Buy products online from china wholesalers at aliexpress.com. `https://www.aliexpress.com/popular/continuous-spo2-monitoring.html`, 2013 (Accessed: 2017- 09- 08).

[7] Medtronic diabetes. Continuous Glucose Monitoring. `https://www.medtronicdiabetes.com/treatments/continuous-glucose-monitoring`, 2013 (Accessed: 2017- 09- 02).

[8] Atallahco. Electrocardiograph / ECG Monitor. `http://www.atallahco.com/index.php/monitor-electrocardiograph-ecg-monitor-c-2_379_388`, 2013 (Accessed: 2017- 08- 22).

[9] playstation. PS4. `https://www.playstation.com/en-us/explore/ps4/`, 2013 (Accessed: 2017- 08- 22).

[10] J Patrick Reilly. *Applied bioelectricity: from electrical stimulation to electropathology*. Springer Science & Business Media, 2012.

[11] Maulin Patel and Jianfeng Wang. Applications, challenges, and prospective in emerging body area networking technologies. *IEEE Wireless communications*, 17(1), 2010.

[12] Arsalan Mosenia, Susmita Sur-Kolay, Anand Raghunathan, and Niraj Jha. Wearable medical sensor-based system design: A survey. *IEEE Transactions on Multi-Scale Computing Systems*, 2017.

[13] WHAT ARE BRAINWAVES? `http://www.brainworksneurotherapy.com/what-are-brainwaves`, 2013 (Accessed: 2017- 09- 08).

[14] The Physics Factbook. Frequency Of A Beating Heart. `https://hypertextbook.com/facts/1998/ArsheAhmed.shtml`, 2013 (Accessed: 2017- 09- 08).

[15] Riccardo Cavallari, Flavia Martelli, Ramona Rosini, Chiara Buratti, and Roberto Verdone. A survey on wireless body area networks: Technologies and design challenges. *IEEE Communications Surveys & Tutorials*, 16(3):1635–1657, 2014.

[16] MirHojjat Seyedi, Behailu Kibret, Daniel TH Lai, and Michael Faulkner. A survey on intrabody communications for body area network applications. *IEEE Transactions on Biomedical Engineering*, 60(8):2067–2079, 2013.

[17] Thoams Guthrie Zimmerman. Personal area networks: near-field intrabody communication. *IBM systems Journal*, 35(3.4):609–617, 1996.

[18] Ruixia Liu, Yinglong Wang, Minglei Shu, and Shangbin Wu. Throughput assurance of wireless body area networks coexistence based on stochastic geometry. *PloS one*, 12(1):e0171123, 2017.

[19] Maria Amparo Callejon, David Naranjo-Hernandez, Javier Reina-Tosina, and Laura M Roa. A comprehensive study into intrabody communication measurements. *IEEE Transactions on Instrumentation and Measurement*, 62(9):2446–2455, 2013.

[20] Takashi Handa, Shuichi Shoji, Shinichi Ike, Sunao Takeda, and Tetsushi Sekiguchi. A very low-power consumption wireless ecg monitoring system using body as a signal transmission medium. In *Solid State Sensors and Actuators, 1997. TRANSDUCERS'97 Chicago., 1997 International Conference on*, volume 2, pages 1003–1006. IEEE, 1997.

[21] Derek P Lindsey, Eric L McKee, Maury L Hull, and Stephen M Howell. A new technique for transmission of signals from implantable transducers. *IEEE transactions on biomedical engineering*, 45(5):614–619, 1998.

[22] Kurt Partridge, Bradley Dahlquist, Alireza Veiseh, Annie Cain, Ann Foreman, Joseph Goldberg, and Gaetano Borriello. Empirical measurements of intrabody communication performance under varied physical configurations. In *Proceedings of the 14th annual ACM symposium on User interface software and technology*, pages 183–190. ACM, 2001.

[23] Michael Oberle. *Low power systems-on-chip for biomedical applications*. PhD thesis, 2002.

[24] Katsuyuki Fujii, Koichi Ito, and Shigeru Tajima. Signal propagation of wearable computer using human body as transmission channel. In *Proceedings of the International Symposium on Antennas and Propagation ISAP-02*, pages 512–515, 2002.

[25] Keisuke Hachisuka, Azusa Nakata, Teruhito Takeda, Yusuke Terauchi, Kenji Shiba, Ken Sasaki, Hiroshi Hosaka, and Kiyoshi Itao. Development and performance analysis of an intra-body communication device. In *TRANSDUCERS, Solid-State Sensors, Actuators and Microsystems, 12th International Conference on, 2003*, volume 2, pages 1722–1725. IEEE, 2003.

[26] Keisuke Hachisuka, Yusuke Terauchi, Yoshinori Kishi, Ken Sasaki, Terunao Hirota, Hiroshi Hosaka, Katsuyuki Fujii, Masaharu Takahashi, and Koichi Ito. Simplified circuit modeling and fabrication of intrabody communication devices. *Sensors and actuators A: physical*, 130:322–330, 2006.

[27] Mitsuru Shinagawa, Masaaki Fukumoto, Katsuyuki Ochiai, and Hakaru Kyuragi. A near-field-sensing transceiver for intrabody communication based on the electrooptic effect. *IEEE Transactions on instrumentation and measurement*, 53(6):1533–1538, 2004.

[28] Marc Simon Wegmueller, Andreas Kuhn, Juerg Froehlich, Michael Oberle, Norbert Felber, Niels Kuster, and Wolfgang Fichtner. An attempt to model the human body as a communication channel. *IEEE transactions on Biomedical Engineering*, 54(10):1851–1857, 2007.

[29] Marc Simon Wegmueller, Michael Oberle, Norbert Felber, Niels Kuster, and Wolfgang Fichtner. Signal transmission by galvanic coupling through the human body. *IEEE Transactions on Instrumentation and Measurement*, 59(4):963–969, 2010.

[30] Jordi Agud Ruiz and Shigeru Shimamoto. Experimental evaluation of body channel response and digital modulation schemes for intra-body communications. In *Communications, 2006. ICC'06. IEEE International Conference on*, volume 1, pages 349–354. IEEE, 2006.

[31] Jordi Agud Ruiz and Shigeru Shimamoto. Statistical modeling of intra-body propagation channel. In *Wireless Communications and Networking Conference, 2007. WCNC 2007. IEEE*, pages 2063–2068. IEEE, 2007.

[32] Meenupriya Swaminathan, Ferran Simon Cabrera, Joan Sebastia Pujol, Ufuk Muncuk, Gunar Schirner, and Kaushik R Chowdhury. Multi-path model and sensitivity analysis for galvanic coupled intra-body communication through layered tissue. *IEEE transactions on biomedical circuits and systems*, 10(2):339–351, 2016.

[33] Kenneth S Cole and Robert H Cole. Dispersion and absorption in dielectrics i. alternating current characteristics. *The Journal of chemical physics*, 9(4):341–351, 1941.

[34] Damijan Miklavčič, Nataša Pavšelj, and Francis X Hart. Electric properties of tissues. *Wiley encyclopedia of biomedical engineering*, 2006.

[35] Sami Gabriel, RW Lau, and Camelia Gabriel. The dielectric properties of biological tissues: Iii. parametric models for the dielectric spectrum of tissues. *Physics in medicine and biology*, 41(11):2271, 1996.

[36] Ahmed E Khorshid, Ahmed M Eltawil, and Fadi Kurdahi. Intra-body communication model based on variable biological parameters. In *Signals, Systems and Computers, 2015 49th Asilomar Conference on*, pages 948–951. IEEE, 2015.

[37] NEVA Electromagnetics. `https://www.nevaelectromagnetics.com/`, 2009 (Accessed: 2017- 09- 08).

[38] Keisuke Hachisuka, Teruhito Takeda, Yusuke Terauchi, Ken Sasaki, Hiroshi Hosaka, and Kiyoshi Itao. Intra-body data transmission for the personal area network. *Microsystem Technologies*, 11(8-10):1020–1027, 2005.

[39] A Ahlbom, U Bergqvist, JH Bernhardt, JP Cesarini, M Grandolfo, M Hietanen, AF Mckinlay, MH Repacholi, David H Sliney, J Stolwijk, et al. Guidelines for limiting exposure to time-varying electric, magnetic, and electromagnetic fields (up to 300 ghz). *Health physics*, 74(4):494–521, 1998.

[40] Kenneth Hoyt, Benjamin Castaneda, and Kevin J Parker. 5c-6 muscle tissue characterization using quantitative sonoelastography: Preliminary results. In *Ultrasonics Symposium, 2007. IEEE*, pages 365–368. IEEE, 2007.

[41] Behailu Kibret, MirHojjat Seyedi, Daniel TH Lai, and Micheal Faulkner. Investigation of galvanic-coupled intrabody communication using the human body circuit model. *IEEE journal of biomedical and health informatics*, 18(4):1196–1206, 2014.

[42] Dr. Nadine James. Intracellular Fluid: Definition and Composition. `http://study.com/academy/lesson/intracellular-fluid-definition-composition.html`, 2016 (Accessed: 2017- 11- 05).

[43] Rife videos. The "Skin Effect" And Bio-Electrical Impedance Analysis . `http://www.rifevideos.com/the_skin_effect_and_bio_electrical_impedance_analysis.html`, (Accessed: 2017- 11- 06).

[44] William T McCartney. *The design, manufacture and analysis of a new implant for fracture fixation in human and veterinary orthopaedic surgery: the bone fastenerod*. PhD thesis, Dublin City University, 2002.

[45] *Dynamic Compression Plates, DCP, 3.5 mm*, 2017 (Accessed: 2017- 06- 15).

[46] Assefa K Teshome, Behailu Kibret, and Daniel TH Lai. Galvanically coupled intrabody communications for medical implants: A unified analytic model. *IEEE Transactions on Antennas and Propagation*, 64(7):2989–3002, 2016.

[47] Ernest L Madsen, Maritza A Hobson, Gary R Frank, Hairong Shi, Jingfeng Jiang, Timothy J Hall, Tomy Varghese, Marvin M Doyley, and John B Weaver. Anthropomorphic breast phantoms for testing elastography systems. *Ultrasound in medicine & biology*, 32(6):857–874, 2006.

[48] Mariya Lazebnik, Ernest L Madsen, Gary R Frank, and Susan C Hagness. Tissue-mimicking phantom materials for narrowband and ultrawideband microwave applications. *Physics in medicine and biology*, 50(18):4245, 2005.

[49] Chung-Kwang Chou, Gang-Wu Chen, Arthur W Guy, and Kenneth H Luk. Formulas for preparing phantom muscle tissue at various radiofrequencies. *Bioelectromagnetics*, 5(4):435–441, 1984.